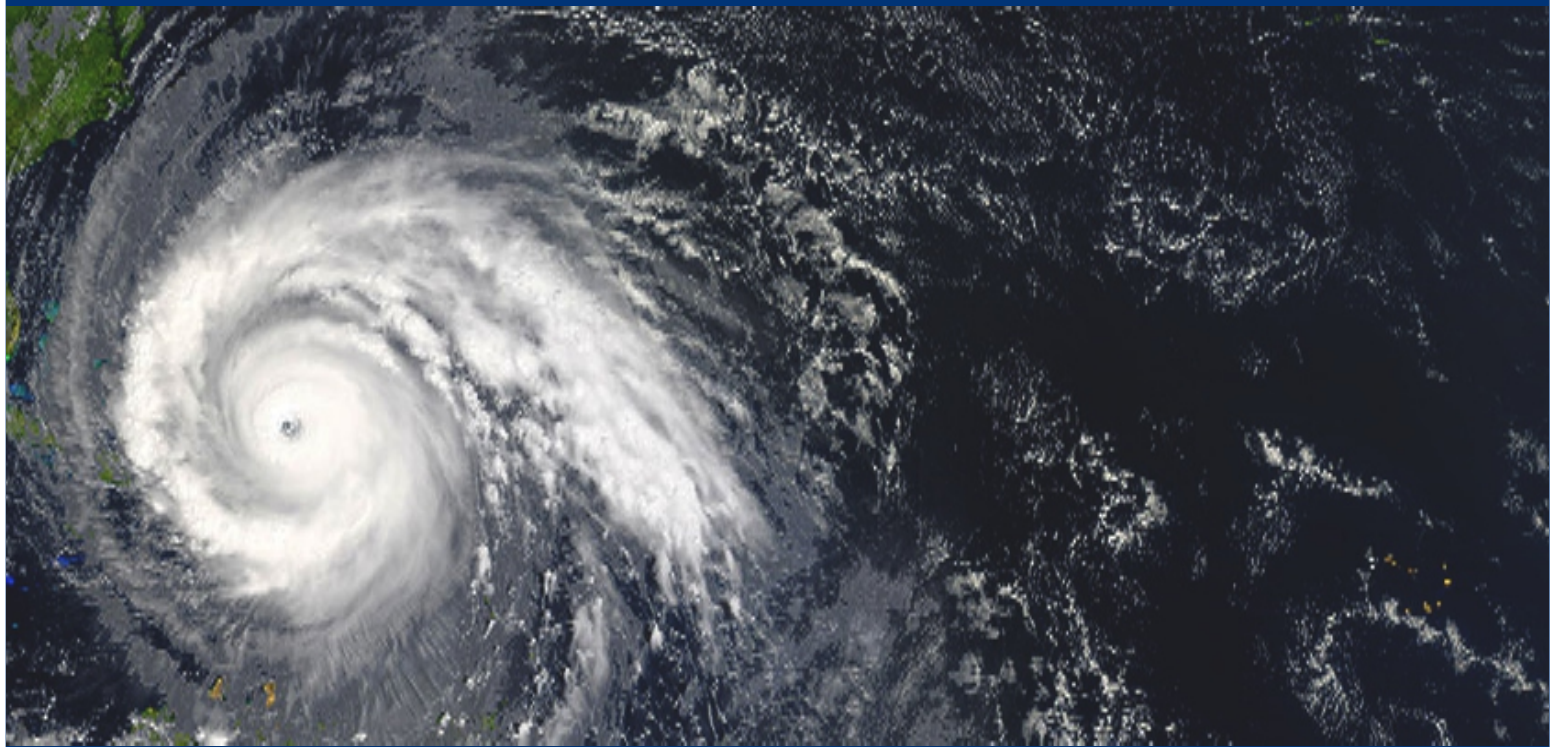


DISASTER SCIENCE AND ENGINEERING



VOL: 6, NO:1, 2020

ISSN: 2149-7249

For more info, you may visit
www.disasterengineering.com



DISASTER SCIENCE AND ENGINEERING
EDITORIAL BOARD
Volume: 6, Issue 1, May 2020

Editor-in-Chief

İnan KESKİN, inankeskin@karabuk.edu.tr

Editors

Emrah DOĞAN, emrahd@sakarya.edu.tr
Haluk AKGÜN, hakgun@metu.edu.tr
Tülay EKEMEN KESKİN, tulayekemen@karabuk.edu.tr
Veysel Harun ŞAHİN, vsahin@sakarya.edu.tr

Editorial Board

Abolfazl Nazari GİGLOU, abolfazl@uidaho.edu
Adem AKPINAR, ademakpinar@uludag.edu.tr
Ali ATEŞ, atesali2000@gmail.com
Ayşe ÇAĞLAYAN, ayse.caglayan@csb.gov.tr
Bagya PACKİALAKSHMĪ, bagyaram@gmail.com
Beytullah EREN, beren@sakarya.edu.tr
Cem KIRLANGIÇOĞLU, kirlangicoglu@sakarya.edu.tr
Cüneyt BAYKAL, cbaykal@metu.edu.tr
Emrah DOĞAN, emrahd@sakarya.edu.tr
Erkan ÇELEBİ, ecelebi@sakarya.edu.tr
Fatih GÖKTEPE, fgoktepe@sakarya.edu.tr
Haluk AKGÜN, hakgun@metu.edu.tr
Tülay EKEMEN KESKİN, tulayekemen@karabuk.edu.tr
Isık YILMAZ, iyilmaz@cumhuriyet.edu.tr
İnan KESKİN, inankeskin@karabuk.edu.tr
İsmail Hakkı DEMİR, idemir@sakarya.edu.tr
Mehmet Fatih DÖKER, fdoker@sakarya.edu.tr
Mehmet İnanç ONUR, mionur@eskisehir.edu.tr
Murat UTKUCU, mutkucu@sakarya.edu.tr
Mustafa Kerem KOÇKAR, mkoçkar@gazi.edu.tr
Osman SÖNMEZ, osonmez@sakarya.edu.tr
Ömer GİRAN, ogiran@istanbul.edu.tr
Selim DOĞAN, sdogan@selcuk.edu.tr
Shivam TRĪPATHĪ, shiva@iitk.ac.in
Soydan SERTTAŞ, soydan.serttas@dpu.edu.tr
Tolga GÖRÜM, tgorum@itu.edu.tr
Veysel Harun ŞAHİN, vsahin@sakarya.edu.tr



Examination of Earthquake Intensity Increments on Side-Zones of Valleys within Alluvial Basins by an Analytical Approach

A. Hakan MUTLU^{1*}, Süleyman PAMPAL², Ünsal SOYGÜR², Alkut AYTUN³

¹ Department of Construction and Real Estate, Ministry of National Education, Ankara

² Department of Civil Engineering, Faculty of Engineering, Gazi University, Ankara

³ Department of Geophysical Engineering, Faculty of Engineering, Ankara University, Ankara

ABSTRACT

The effect of topography on the seismic wave-motion has been of interest to many studies. In this study, the earthquake-intensity increments (amplification) on side-zones of valleys within alluvial basins, were investigated using finite element method. A set of finite element models for valleys, one with a triangular cross-section, and the rest with trapezoidal cross-sections, taking into account five different side slopes (17°, 22°, 27°, 37°, 45°), were adapted. The acceleration time-histories obtained through the use of the commercial finite element code (QUAD4M) at valley-sides, valley-edges, and at the intermediate points were transformed to Fourier Amplitude Spectra. The amplitude-frequency variations obtained at the three selected reference points of the valley as well as at the bedrock, were investigated in each of the four selected phases of the earthquake duration. As a result of the performed dynamic analysis, the effect of the valley-slope variation at the three reference points on the valley was examined at four distinct phases of the earthquake duration.

Keywords: Effects of topography, slope of valley, seismic reflection

1. INTRODUCTION

The fact that the local ground conditions significantly affect the strong earthquake ground- motion is clearly demonstrated by the structural damage and the instrumental measurements observed in devastating earthquakes [1]. Therefore, it can be stated that local ground conditions should be considered in the design of earthquake-resistant structures. The increase in the amplitude of the earthquake-waves, passing through the surface layers, is known as soil amplification. Ground conditions, such as bedrock depth, thickness of the soil layers on the bedrock, their types and dynamic characteristics, changes with depth and deformation, lateral discontinuity of the soil layers, and topographic characteristics, are all important factors affecting the soil amplification. The topographic features include the geometry of the bedrock, which is bounded by the two- or three- dimensional geometry of the ground layers on and under the surface [2].

*Corresponding Author: is ahmethakanmutlu@gmail.com

Stemming from the cyclic character of the earthquake-waves, formed on the surface of the sloping bedrock, surface-waves running towards the valley-center are generated [3]. These waves produce strong and long-lasting ground motions which cannot be predicted by one-dimensional analysis, based on the dynamic behavior of the ground layers under vertically ascending shear-waves. The ordinates of the long-period side of the spectrum increases, from the edge to the center of the valley, while in critical localities, maximal effects of two-dimensional magnification show up [4].

The surface-waves formed on the edges of the plain, as a result of lateral confinement of loose soil layers, dominate after a certain distance, as they advance through the plain. Surface-waves have lower velocities than the waves formed in three-dimensional environments and have periods greater than 0.5 seconds. If the plain is very wide, it is observed that these waves disappear due to damping effect of the ground. In the case of a narrow valley within an alluvial environment, such surface-waves have been clearly observed in a number of earthquakes, during which the ground-motion has undergone significant changes at the surface, due to multiple reflection of the waves, to-and-fro the rock surface, bounding the valley [5]. Surface topography too, has always been considered as a major factor, affecting the ground-motion. Chaljub et al. concludes that, this is significant in elevated areas; however, they found it less important in the valleys [6]. Lovati et al. evaluated the seismic site response of Narni ridge (central Italy), by comparing experimental results with those from numerical simulations [7]. Barani et al. examine the role of topographic effects on the earthquake ground-motion. However, they attribute little importance to the effects of topography, which, as known, may play a significant role on the level, duration and frequency content of ground-motion [8].

Alielahi et al. make an attempt to study the effect of U-shaped canyon-cavity geometry on strong ground-motion. They performed response analysis for different sizes of a U-shaped canyon, in the presence of differently positioned underground cavities. The results showed that the response is strongly influenced by the size of U-shaped canyon [9]. The earth's surface-irregularities can substantially affect seismic-waves and induce amplifications of ground motions. Ning et al. investigated whether and how the source characteristics affect the site-amplification effects. They proposed an analytical model of a line source of cylindrical waves impinging on an alluvial valley, to link the source and the site. The analytical solution to this problem proves one aspect of the strong effect of source on site amplification, i.e., the wave-curvature effect. They found that the site amplification depends on the source location, especially under conditions of a small source-to-site distance [10].

Khan et al. investigated the influence of ground-surface topography on the spatial distribution of earthquake-induced ground shaking. This study shows the influence of topography on seismic amplification during the 2005 Kashmir earthquake. Earth-surface topography scatters and reflects seismic-waves, causing spatial variation in seismic response. A 3D simulation has been performed for the 2005 Kashmir earthquake in Muzaffarabad, with spectral finite- element method. The moment-tensor solution of the 2005 Kashmir earthquake is used as the seismic source. The results point to amplification of seismic response on ridges and de-amplification on valleys. It is found that slopes facing away from the source receive an amplified seismic response, and that 98% of the highly damaged areas are located in the topographically amplified seismic response zone [11].

Iyisan et al. pointed to the fact that earthquake ground-motion is affected by the local soil conditions, geological structures, as well as earthquake source properties. The amplitude and frequency content of the strong ground-motion can be substantially modified by local site effects. They investigated the effects of basin-edge on the variation of surface-motion using different strong ground-acceleration record, performed one and two dimensional dynamic analyses, employing the Dinar basin-edge model, and compared the results [12].

The aim of this study is to evaluate the ground-motion changes numerically, at a set of three reference points chosen along the axis of the valley, for different valley-slopes, by applying the finite-element method. The starting point of this study stems from the engineering interest in view of determining the causes of the heavy damage in the Çay Small Industrial Area (Çay Küçük Sanayi Sitesi), due to the earthquakes in Afyon, on 03.02.2002, and determining whether the topographical structure of the region showed similar aspects to the topographic conditions observed in the studies, mentioned above. As a result of the examination, the geotechnical and geological reasons of the damage, that played an important role in Çay Small Industrial Area, during 2002 Çay Earthquake, were revealed and the issue of seismic refraction and reflection was clearly addressed [13].

2. MATERIALS AND METHODS

On 03.02.2002, an earthquake occurred near Afyon at 09:11 AM. The location and the magnitude of this earthquake were determined differently by various recording stations. It is thought that the earthquake that occurred later, was not an aftershock but a second independent earthquake, related to a different fault. It is stated that the epicenter of the second earthquake is between Çay and Maltepe. The second earthquake occurred at 11:55 AM local time and the magnitudes were determined as $M = 6,5$ and $M = 6,0$ respectively. In this study, 03.02.2002 Eber (Sultandagi) - Çay Earthquake data were used and a set of finite element models were adopted, taking into account five different valley-slopes (17° , 22° , 27° , 37° , 45°), one of them with triangular, and the others with trapezoidal sections. The acceleration time-histories obtained at a point on valley-edge, at a point on the valley-axis and at a point between them, were all transformed into Fourier Amplitude Spectra with the computer program (QUAD4M). The amplitude-frequency variations on the selected three points and on the bedrock are divided into four phases and examined independently. For the four different phases of the earthquake duration, the effect of valley slope-changes in these three different points on the valley has been studied by dynamic analysis.

3. RESULTS

QUAD4M is a program, developed on the basis of plane-strain and used for two-dimensional dynamic analysis in x and y directions. In the program, which is not in the upright direction (z) to the plane, the angle of the valley edge was selected as a variable and dynamic analyses were made for five different angles (17° , 22° , 27° , 37° , 45°). As a result, the horizontal accelerations at points A, B and C in Figure 3.1 were obtained, as a function of time. In all the models, the valley is divided into two by taking the advantage of symmetry principle, between the valley-edge and the valley-axis of 2000 m (2 km), and the depth of the alluvium section being 600 m.

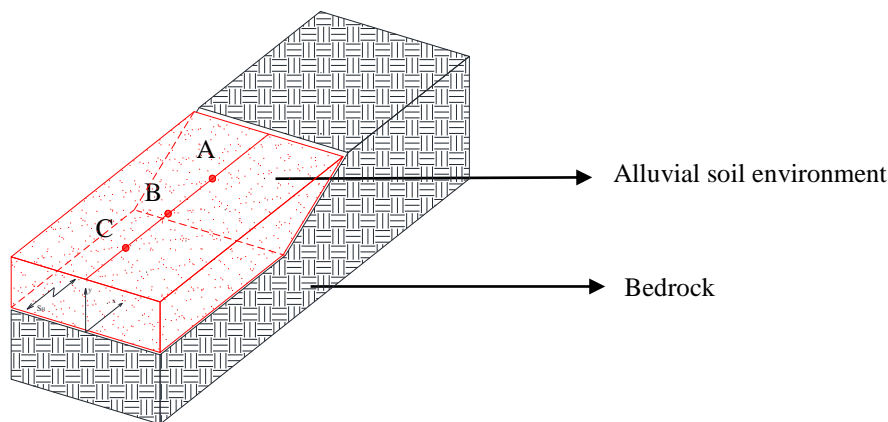


Figure 3.1. Cross-section view of three-dimensional valley

For the QUAD4M program used in the dynamic analysis, the alluvial soil environment of the three-dimensional valley shown in Figure 3.1 is divided into finite-elements (Figure 3.2), a horizontal (x direction) time-varying earthquake force was applied at the interface. Thus, it was thought that the earthquake-waves, emerged from the earthquake-source, as occurred in the nature, climb upwards in the bedrock, can be represented with a more accurate approach.

After the earthquakes on 03.02.2002, the ground data obtained from the studies in the field of application, which can be used in dynamic analysis, are given below:

Unit weight (γ) = 19,4 kN/m³, Shear Modulus (G) = 5.550 kN/m², Shear Modulus Ratio = 0,6 G_{max} , Poisson Ratio (ν) = 0,35 and Elasticity Modulus (E_s) = 25.000 kN/m²

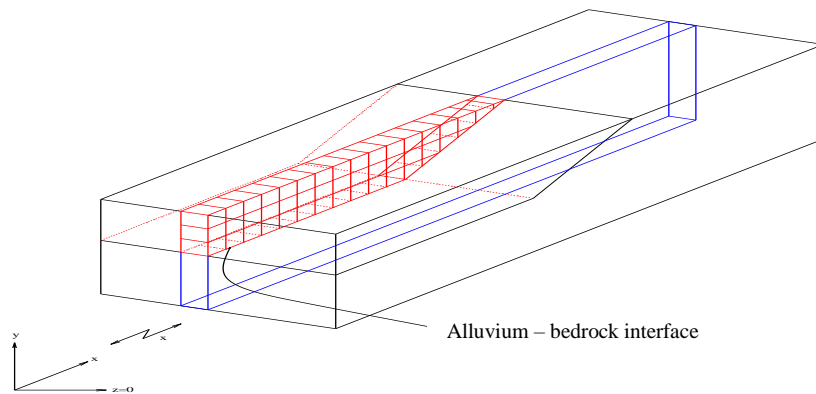


Figure 3.2. Representation of finite-element model, applied to alluvial-basin valley.

The acceleration record of the earthquake, occurred on 03.02.2002, are divided into four phases as shown in Figure 3.3. Since no change could be observed in the first 20 seconds, the stages are listed from the 20th second on.

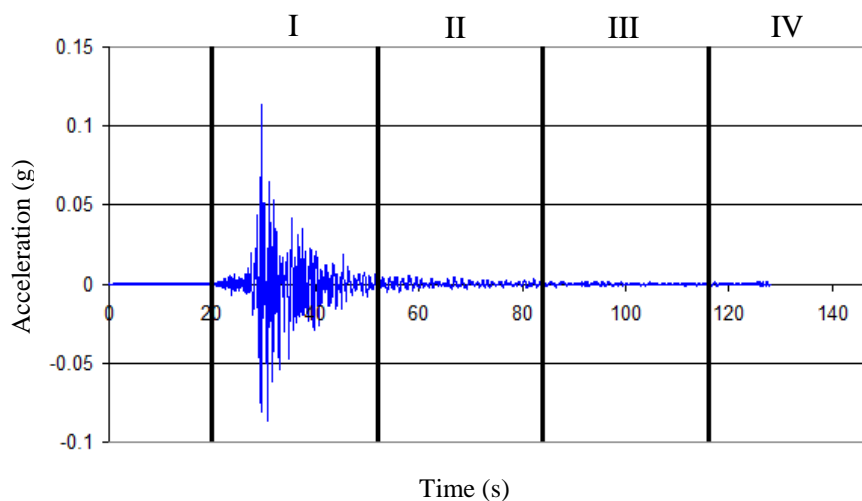


Figure 3.3. Afyon - Sultandağı earthquake acceleration record.

Fast Fourier Transformation (FFT) was performed for each stage of the acceleration record, examined in four stages and shown in Figure 3.4 (a, b, c, d).

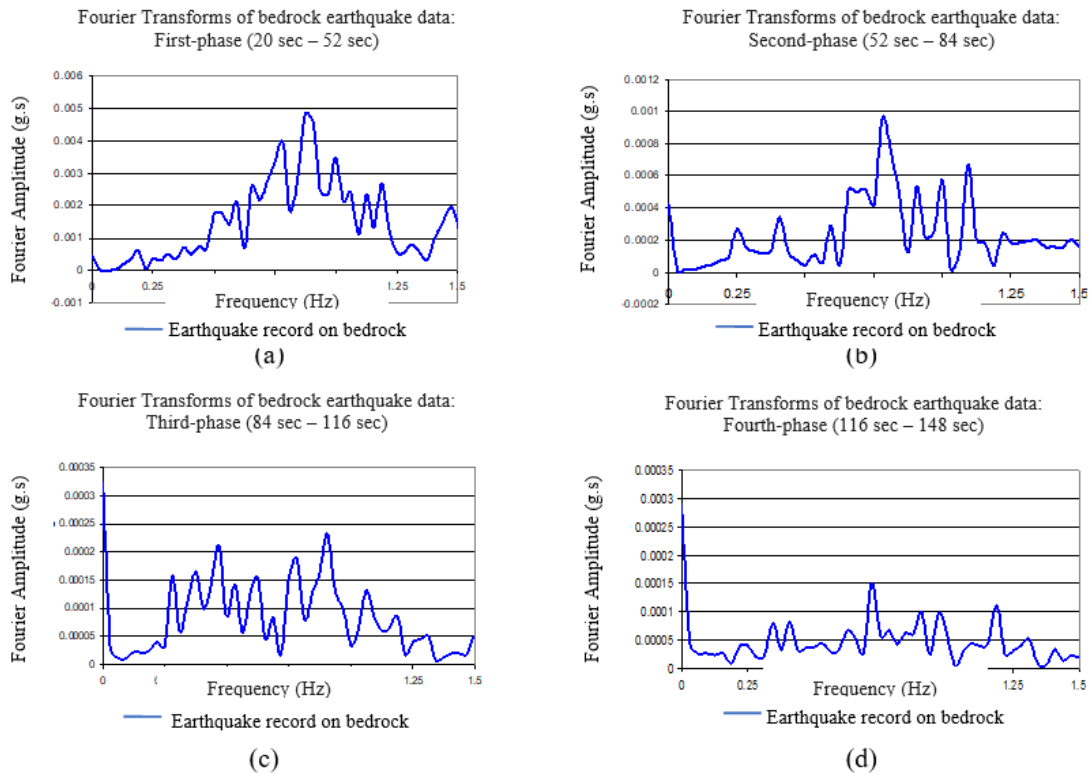


Figure 3.4. Fourier Transforms of four different phases of bedrock earthquake data; (a) First-Phase, (b) Second-Phase (c) Third-Phase, (d) Fourth-Phase.

Considering the explanations above, it is possible to divide the time during which the data takes place, including the acceleration time-histories in the bedrock, as well as the points A, B and C, in four stages of 4096 points (32 seconds), since the number of points $4096 = 2^{12}$ is in accordance with the approach in Fourier Analysis. For this reason, the acceleration time- histories on both the bedrock and at points A, B and C were divided into four time periods, each consisting of 4096 points (32 seconds), with minor modifications, required to start from zero for each phase, and end in zero. Thus, FFT processing conditions were also met.

In this way, it is possible to assume the earthquake-duration as comprised of four stages and to make the interpretations in a more comprehensive way. The amplitude-frequency composition of the earthquake is thus assumed to change by time. In addition, it was observed that the re-expression of data in four time-periods of 4096 points led to meaningful and consistent results [14].

3.2. First Model

The above-mentioned program is implemented on a 17° inclined model. In this model, a semi-equilateral triangular alluvium layer is divided into finite elements. This model can also be considered to represent the low-slope canyon.

From the valley axis to 1800th m (A), 900th m (B) and 100th m (B) (respectively 167th, 67th and 9th nodes) as a result of the dynamic analysis of the FFT applications are given below with the bedrock earthquake-data.

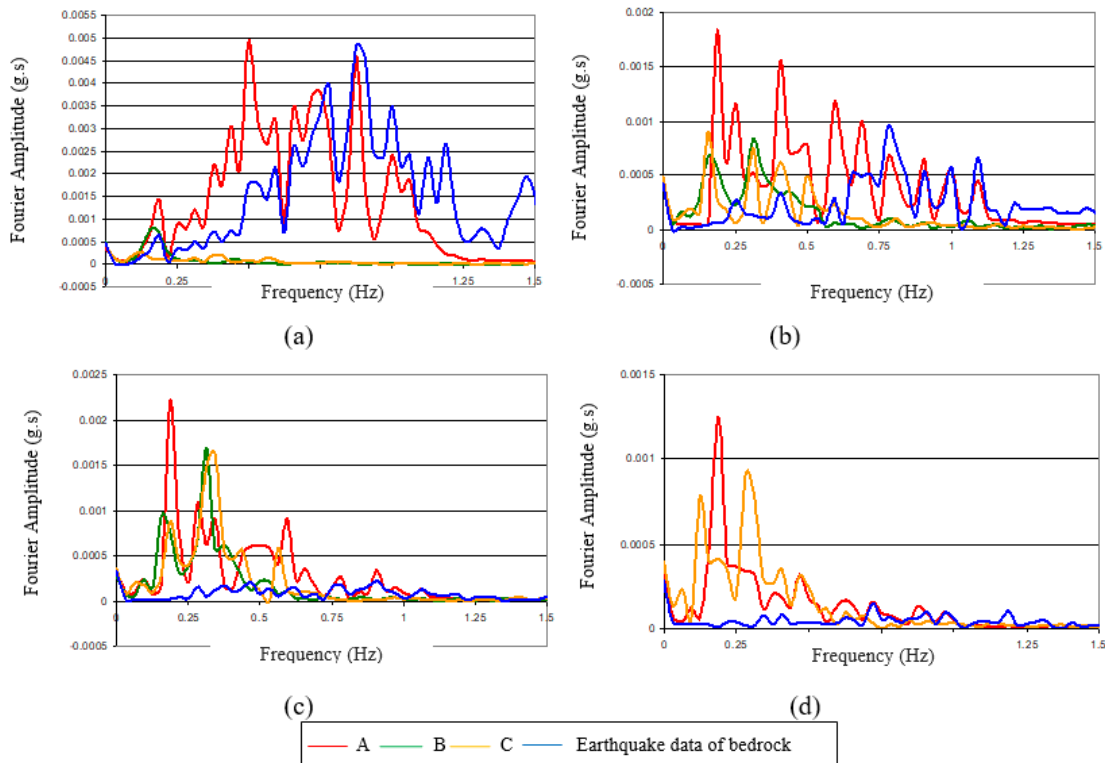


Figure 3.5. (a) Valley slope: 17°; First-Phase; between 20th second and 52th second.
 (b) Valley slope: 17°; Second-Phase; between 52th second and 84th second.
 (c) Valley slope: 17°; Third-Phase; between 84th second and 116th second.
 (d) Valley slope: 17°; Fourth-Phase; between 116th second and 148th second.

It has been determined that point A reached the highest values, especially at low frequencies in all stages and that the amplitudes diminished quantitatively over time. It was observed that points B and C generally exhibit the same behavior and that they coincide with that of the second phase, for the bedrock amplitudes, but never reached the amplitude of point A.

3.3. Second Model

In this case, the finite element network was drawn by taking the slope of the valley at 22° and the dynamic parameters adopted in the first model were repeated.

From the valley axis to 1800th m (A), 900th m (B) and 100th m (B) (respectively 172nd, 82th and 10th nodes) as a result of the dynamic analysis of the FFT applications are given below with the bedrock earthquake-data.

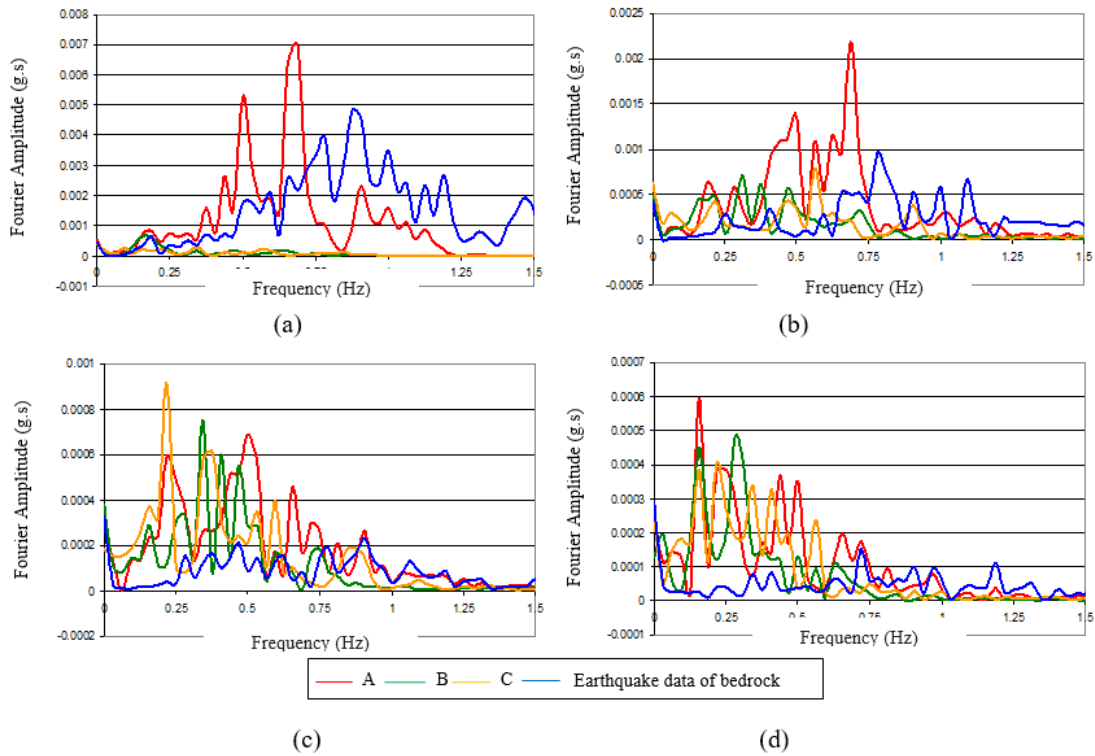


Figure 3.6. (a) Valley slope: 22°; First-Phase; between 20th second and 52th second.
 (b) Valley slope: 22°; Second-Phase; between 52th second and 84th second.
 (c) Valley slope: 22°; Third-Phase; between 84th second and 116th second.
 (d) Valley slope: 22°; Fourth-Phase; between 116th second and 148th second.

In the Second Model, it was determined that point A reached the highest values especially at low frequencies, in almost all stages, and that the amplitudes diminished quantitatively. It was observed that the points B and C generally exhibit a similar behavior and were above the bedrock amplitudes in the second phase. However, unlike the first model, the points B and C were found to pass the amplitude of point A, quantitatively, in the third stage.

3.3. Third Model

In this model, the slope of the valley is 27°, so it is steeper than those of the first two models.

From the valley axis to 1800th m (A), 900th m (B) and 100th m (B) (respectively 181th, 55th and 10th nodes) as a result of the dynamic analysis of the FFT applications are given below with the bedrock earthquake-data.

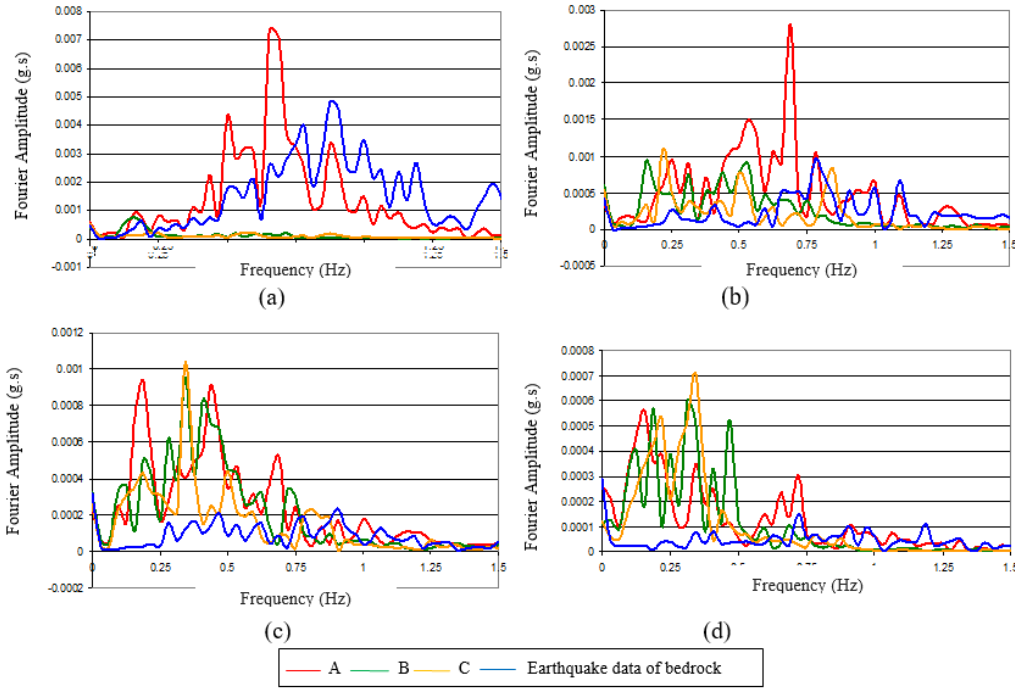


Figure 3.7. (a) Valley slope: 27°; First-Phase; between 20th second and 52th second.
 (b) Valley slope: 27°; Second-Phase; between 52th second and 84th second.
 (c) Valley slope: 27°; Third-Phase; between 84th second and 116th second.
 (d) Valley slope: 27°; Fourth-Phase; between 116th second and 148th second.

In the third model, similar results were obtained as in the second model. It was observed that point A amplitudes reached the highest values, except the third stage at low frequencies.

3.4. Fourth Model

In this model, the slope of the valley was 37° and results were obtained accordingly. From the valley-axis to 1800th m (A), 900th m (B) and 100th m (B) (respectively 159th, 65th and 9th nodes) as a result of the dynamic analysis of the FFT applications are given below with the bedrock earthquake-data. In this model, it has been determined that, with the increase of the angle of the valley slope, there have been decreases in the amplitudes of point A which reached very high amplitudes at low frequencies than those of the other three models. On the contrary, there were increases in the amplitudes at the points B and C, between the valley-axis and the valley-edge.

3.5. Fifth Model

Finally, the valley-slope was selected as 45°, and the results were compared with those from other models. From the valley axis to 1800th m (A), 900th m (B) and 100th m (B) (respectively 700th, 172nd and 20th nodes) as a result of the dynamic analysis of the FFT applications are given below with the bedrock earthquake-data. Fifth model was shown to be similar in frequency-fourier amplitude of the fourth model, it has been determined that there was a decrease in the amplitudes of point A, and increase in the amplitude of points B and C. As a result, the critical region shifts from the valley corner to the middle of the valley, as the valley angle of inclination increases. This situation is in accordance with the study by Cılız, 2007.

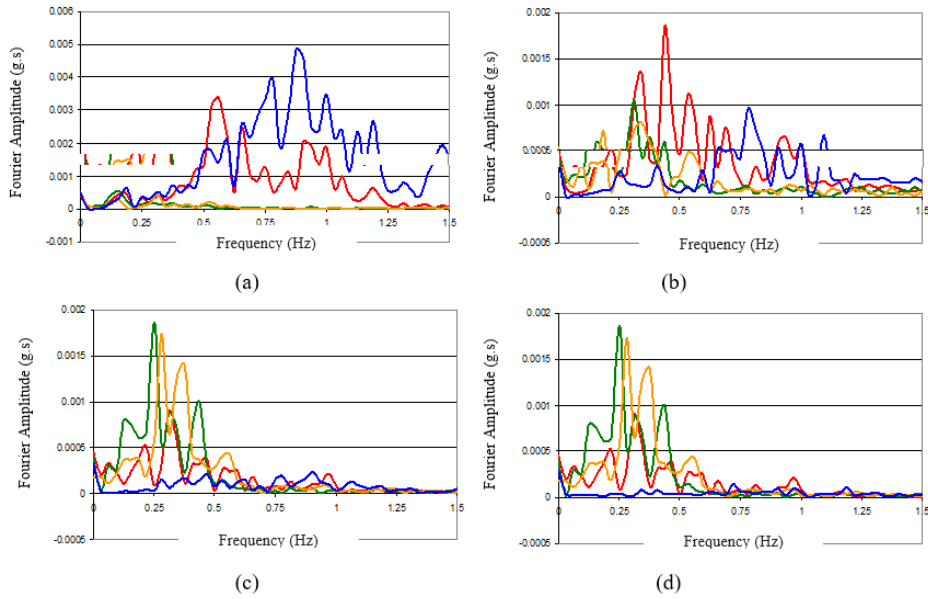


Figure 3.8. (a) Valley slope: 37°; First-Phase; between 20th second and 52th second.
 (b) Valley slope: 37°; Second-Phase; between 52th second and 84th second.
 (c) Valley slope: 37°; Third-Phase; between 84th second and 116th second.
 (d) Valley slope: 37°; Fourth-Phase; between 116th second and 148th second.

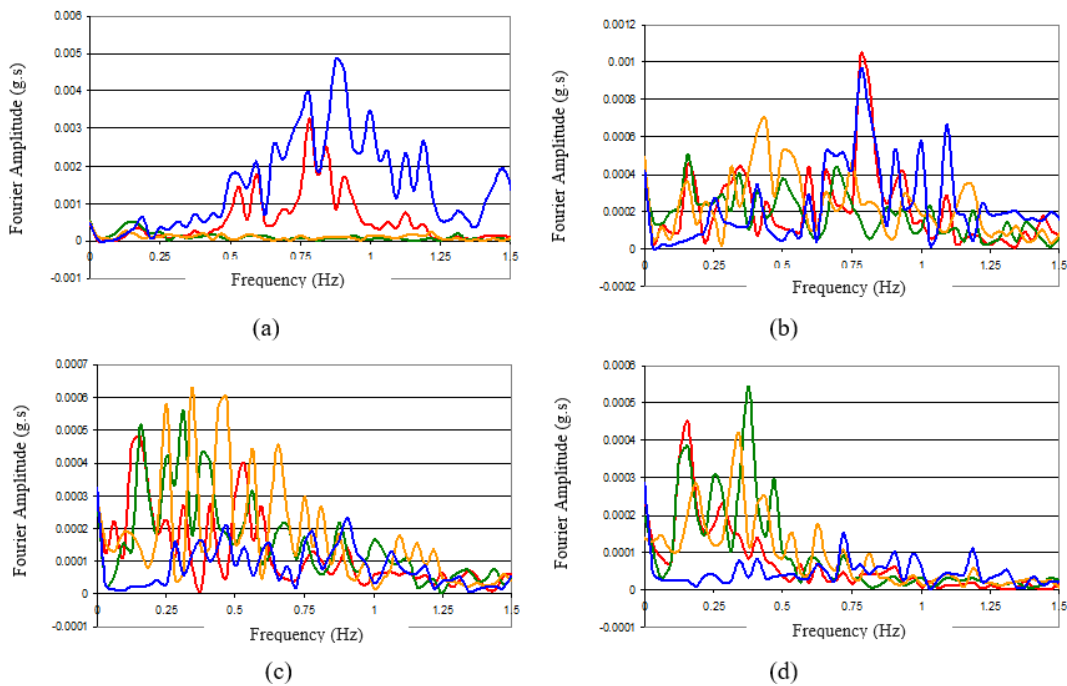


Figure 3.9. (a) Valley slope: 45°; First-Phase; between 20th second and 52th second.
 (b) Valley slope: 45°; Second-Phase; between 52th second and 84th second.
 (c) Valley slope: 45°; Third-Phase; between 84th second and 116th second.
 (d) Valley slope: 45°; Fourth-Phase; between 116th second and 148th second.

4. CONCLUSION

When the acceleration time-histories at the points A, B and C are examined visually, it can be seen that the region at point A near the valley is the most unfavorable locality. The Fourier Amplitude Spectra of the acceleration time-histories obtained at the bedrock and at the three points on the valley-surface ensured a quantitative evaluation of this interpretation.

For Finite Element Analysis, valleys were modeled for five different slopes (17°, 22°, 27°, 37° and 45°), Fourier Amplitude Spectra were obtained from a dynamic analysis with QUAD4M program for three points at side of the valley (A), valley-axis (C) and the intermediate zone (B). Taking three different points for five different angles of inclination, as well as considering the earthquake effect, not as a result of its total duration, but in terms of distinct phases, can be regarded as innovations, brought by this study.

Although the representative earthquake, taken in the study, exhibits a total duration of 128 seconds, its effects vary within certain divisions. These differences can be linked to a phase-specific frequency-amplitude combination.

Since point C corresponds to the deepest part of the valley, this is the place where the effect of frequency (or period, vice-versa) is most likely to be expected. Here, it is expected that the magnified effect of the earthquake-wave components at the ground, the prevailing frequency will be observed and the components at lower and higher frequencies will be weakened, as seen as a result of the analyses. The simple waves in the sine form were able to preserve their visible and recognizable forms, around this point.

An intuitive mind could expect the occurrence of a multitude of reflections and overlaps (superposition) at point A, beforehand. Although there is no physical clue for the presence of such a mechanism, the digital results, especially in low-slope conditions, point to the inappropriateness more than the other two points (B and C), in terms of amplitude increments at lower frequencies, and conforming to actual damage distributions encountered in real earthquakes in nature. In summary, the existence of the aforementioned mechanism is not obtained by an intervention that imposes on the lines of calculation, but as an indirect interpretation.

At point B, for the points between the A and C, it is seen that it conforms to the phenomena observed in nature and that it can be assumed as a control point to check the consistency of the results.

Another result, achieved by the finite element analysis with QUAD4M program, is: It is determined that the amplitude increases in the valley-side regions as the valley slope angle increases. This situation coincides with the conclusions of [15], as mentioned above.

5. REFERENCES

- [1] Özyaydın, K., “Yer hareketleri üzerinde yerel zemin koşullarının etkisi ve zemin büyütmesi”, *TDV*, TDV/TR 96-003, İstanbul, 2-6 (1996).
- [2] Haşal, M., İyisan, R., “Yerel zemin koşullarının zemin büyütmesine etkisi: bir ve iki boyutlu analiz, *ZM 10 Kongresi*, İstanbul, 343-352 (2004).
- [3] Şafak, E., “Local site effects and dynamic soil behaviour”, *Soil Dynamics and Earthquake Engineering*, 21: 453-458 (2001).

- [4] Rassem, M., Ghobarah, A., Heidebrecht, A.C., “Engineering perspective for the seismic site response of alluvial valleys”, *Earthquake Engineering and Structural Dynamics*, 26: 477-493 (1997).
- [5] Bakır, B.S., Erşahin, B., “Alüvyon Vadi ve Havzalarında Gömülü Topografyanın Kuvvetli Yer Hareketi Üzerindeki Etkileri”, *4. Ulusal Deprem Mühendisliği Konferansı*, ODTÜ Kongre ve Kültür Merkezi, Ankara, 79-87 (1997).
- [6] Chaljub E., Moczo P., Tsuno S., Bard P.Y., Kristek J., Käser M., Stupazzini M., Kristekova M., Quantitative Comparison of Four Numerical Predictions of 3D Ground Motion in the Grenoble Valley, France, *Bulletin of the Seismological Society of America*, Vol. 100, No. 4, pp. 1427–1455, August 2010, doi: 10.1785/0120090052
- [7] Lovati, S., Bakavoli, M.K.H., Massa, M., Ferretti, G., Pacor, F., Paolucci, R., Haghshenas, E. & Kamalian, M., Estimation of topographical effects at Narni ridge (Central Italy): comparisons between experimental results and numerical modelling, *Bulletin of Earthquake Engineering*, 9, 2011.
- [8] Barani S., Massa M., Lovati S., Spallarossa D., Effects of surface topography on ground shaking prediction: implications for seismic hazard analysis and recommendations for seismic design, *Geophysical Journal International*, 197, 1551–1565 (2014), doi: 10.1093/gji/ggu095
- [9] Alielahi H., Karimkhani P., Adampira M., Seismic Response of U-shaped Canyon in Presence of Underground Cavity Using BEM, *6th International Conference on Earthquake Geotechnical Engineering*, 1-4 November 2015, Christchurch, New Zealand.
- [10] Ning Z., Yufeng G., Jie Y., Changjie X., An analytical solution to the scattering of cylindrical SH waves by a partially filled semi-circular alluvial valley: near-source site effects, *Earthquake Engineering and Engineering Vibration*, Vol. 14 No 2, 189-201, 2015, DOI:10.1007/s11803-015-0016-3.
- [11] Khan S., Meijde M., Werff H., Shafique M., The impact of topography on seismic amplification during the 2005 Kashmir Earthquake, *Natural Hazards Earth System Science Discussions*, 2019, <https://doi.org/10.5194/nhess-2019-13>.
- [12] İyisan R., Haşal M.E., The Basin Edge Effect on Dynamic Response: Dinar Basin Model, Digest 2011, *Teknik Dergi*, Vol. 22, No 110, 1499-1518, 2011.
- [13] Pampal, S., Soygür, Ü., Mutlu, A.H., “The impact of topography on Çay Small Scale Industrial Complex earthquake damages inflicted by 03.02.2002 Eber (Sultandağı) and Çay Earthquakes”, *ZM 2003*, Lefkoşa, K.K.T.C, 207-213 (2003).
- [14] Mutlu, A.H., “Examination of Earthquake Intensity Increments in Side Zones of Valley with Alluvial Basins by an Analytical Approach and a Model Experiment”, Doktora Tezi, *Gazi Üniversitesi Fen Bilimleri Enstitüsü*, Ankara, 2008.
- [15] Cılız, S., “The Effect of Basin Edge Slope on the Dynamic Response of Soil Deposits”, Doktora Tezi, *ODTÜ Fen Bilimleri Enstitüsü*, Ankara, 2007.



Earthquake Performance Based Design And Resilience Based Analysis in High-Rise Buildings

Ali Dedeoğlu^{1,*}, Abdullah Can Zülfikar², Cüneyt Tüzün³

¹Graduate Student, Civil Engineering / Gebze Technical University, Gebze, Kocaeli, Turkey

²Asst.Prof., Civil Engineering / Gebze Technical University, Gebze, Kocaeli, Turkey

³Instructor, Civil Engineering / Gebze Technical University, Gebze, Kocaeli, Turkey

ABSTRACT

In general, in the design of high-rise buildings performance-based designs and analyzes are carried out using traditional methods. This study suggests performing new generation risk assessment analyzes for high-rise buildings including not only structural risk but also the time and cost related loss that may occur due to non-structural elements after a potential earthquake. The study will provide useful information on the assessment of the economic loss of high-rise buildings after a potential earthquake. The methods and measures taken during the traditional design process, their benefits, the new solutions and alternatives will be assessed. Until recently, the 'Performance Based Design' of structures was the first thing coming to mind in the earthquake risk assessment. However, nowadays the questions on resilience, potential economical and time losses in possible future earthquakes and how these possible losses can be prevented are raised.

In this study, in addition to the performance-based design analysis, FEMA P-58-1 (2012) method which is one of the seismic evaluation methods including assessment of non-structural elements, time and financial loss analysis was used. Within the scope of the study, the fragility curves available in FEMA P58 were used and probabilistic results were obtained about the repair cost, repair time, injuries and insurance costs of the building.

It is believed that the results of this study will be valuable for building owners, managers, insurance companies and risk management. The TBDY 2018 regulation allows us to predict the expected behavior of structural members during a possible earthquake, but nowadays building managers, owners and employers demand more than that. This reveals the need of new generation risk assessment including time and financial loss assessment.

Although the structural system has a significant impact on the seismic performance of the entire building, its cost is only 20% of the total building cost in general. So, the seismic performance should be evaluated in a broader context by the structural engineers not only evaluating the structural elements but also all the systems in the building. The FEMA P-58 (2012) method evaluates the seismic performance of an entire building with a new generation risk assessment tool in terms of loss of life, facility repair cost and repair time in a possible scenario earthquake.

The current study includes the application of new generation risk assessment tool for a 28 floors typical residential high-rise building with the evaluation of seismic performance of non-structural elements, recovery time and related financial loss analysis in addition to the performance based design analysis carried out according to the Turkey Building Earthquake Code (2018).

Keywords: Assessment of earthquake Performans, Nonstructural components, Structural components, İstanbul, High Rise Building,

ÖZET

Bu çalışma, geleneksel yöntemlerle performansa dayalı tasarım ve analizleri yapılan yüksek bir binanın yeni nesil risk değerlendirme analizleri yapılmasını kapsamaktadır. Çalışma sadece yapısal riski değil aynı zamanda potansiyel bir deprem sonrası yapısal olmayan elemanlardan dolayı oluşabilecek riski, zaman ve maliyet kaybını da içerir.

Çalışma bu yönü ile yüksek katlı yapıların deprem sonrası performanslarının ekonomiye olan maliyetinin hesaplanması konusunda oldukça faydalı bilgiler sağlayacaktır. Böylelikle bina tasarımı sırasında ele alınan yöntem ve önlemlerin ne oranda gerekli olduğu, yarar ve fayda dengesi ile yeni çözüm öneri ve alternatiflerinin aranması söz konusu olacaktır. Afet risk yönetimi hakkında yapılan tartışmalarda ilk akla gelen yapıların "Performansa Dayalı Tasarımıdır". Yapıların gelecekteki olası büyük depremlerde doğal tehlikelere karşı daha dayanıklı olmasını nasıl sağlarız ve olası kayıpları nasıl önleyebiliriz gibi sorular artık gündeme gelmektedir.

*Corresponding Author: is alidedeoglu@gtu.edu.tr

Bu çalışmada, Performansa dayalı tasarım sonrasında yapısal olmayan elemanlar, süre ve maliyet kayıp analizlerini de içine alan sismik değerlendirme yöntemlerinden biri olan FEMA P-58-1 (2012) yöntemi kullanılmıştır. Çalışma kapsamında FEMA P58’de mevcut olan kırılma eğrileri kullanılmış ve yapının onarım maliyeti, onarım süresi, yaralanmalar ve sigorta maliyeti hakkında olasılıksal sonuçlar elde edilmiştir. Bu çalışmanın sonuçlarının, bina sahipleri, yöneticileri, sigorta firmaları ve risk yönetimi için değerli olacağına inanmaktayız. TBDY 2018 deprem yönetmeliği olası bir deprem sonrasında yapısal elemanlarda beklenen davranışı tahmin etmemizi sağlamaktadır. Ancak işletmeciler, işverenler ve yapı sahipleri artık bundan daha fazlasını talep etmektedir. Yeni nesil yönetmeliklerin içeriğine, olası deprem sonrasında maliyet ve süre kayıpları analizlerinin de eklenmesi gerektiği ortaya çıkmaktadır.

Yapısal sistem, eklentilerde dâhil olmak üzere tüm binanın sismik performansı üzerinde önemli bir etkiye sahip olmakla birlikte, toplam bina maliyetinin yaklaşık %20’sidir. Bu nedenle, yapı mühendisleri sismik performansı sadece yapısal öğeler ve can güvenliğini sağlayacak önlemlere değil binanın tüm sistemlerine bakarak daha geniş bir bağlamda görmeli ve değerlendirmelidir. FEMA P-58 (2012) yöntemi olası bir deprem senaryosunda can kaybı, tesis onarım maliyeti ve onarım süresi açısından tüm bir binanın sismik performansını değerlendirebilmekte, yeni nesil performansa dayalı sismik tasarım yöntem ve araçlar ile sorgulanabilir metrik cevaplar verebilmektedir.

Bu çalışma, Türkiye Deprem Bina Yönetmeliğinde (2018) yer alan performansa dayalı tasarım ilkelerine dayanarak tasarlanan yüksek (28) katlı tipik bir konut (rezidans) binası için yapısal olmayan elemanların, süre ve maliyet kayıplarının da yer aldığı sismik değerlendirme yönteminin uygulamasını içerir.

Keywords: Performans analizi, Yapsısal elemanlar, Yapısal olmayan elemanlar, Hasar, Yüksek Bina, İstanbul

1. Introduction

Recently, high-rise buildings are designed and built increasingly in Turkey. However, during the design stage of these buildings, the common question is how these buildings will continue to serve to the residents after a potential major earthquake. Many problems are encountered in the design process. As the buildings height increase, the structural system must cope with the two important issues. One of them is wind and the other is earthquake. Design engineers managed to win the struggle with these two issues in some extent with the development of dynamic isolation technology and one by one model building tests. However, how the buildings will continue to serve after the earthquake, how and how these will be reflected to the investor were not much thought. In the literature, especially in the recent years there are several studies on the post-earthquake building use performance studies. Traditionally, the structural system of all high or not high buildings in Turkey is formed from reinforced concrete shearwalls and frames. There is a new earthquake regulation that came into force on 1 January 2018 in Turkey for the design of tall buildings under a possible earthquake (TBDY 2018). In addition, the international resource “Tall Buildings Initiative” (TBI), 2010 is also used. These regulations require the application of performance-based design principles for tall buildings and also require the structural system to be designed by nonlinear time history analysis.

When we look at the building stock in our country and the new buildings under construction, we observe that there is a very intense construction. Most of the buildings that comply with the regulations are designed to provide life safety, not to prevent injuries, limit damage or ensure rapid regeneration. For example, in the new earthquake regulation, it is required to provide “Controlled Damage” performance level at DD-2 level, also called “design earthquake”. Controlled Damage is defined as the level of damage that is not too heavy and mostly repairable, in order to ensure life safety in the regulation. The main task of the design engineer is to ensure life safety in the building. However, the expectations of people from an engineer are far above them. Terms such as durability, planning and preparation, post-disaster use are becoming increasingly important elements for building owners. Therefore, regulations were conducted to analyze the state of the buildings after the earthquake. One of these studies, the USRC Rating System, calculates the building residence and removes important missing information to assist those using the structure, planners, building owners and insurers.

In this study, it is aimed to present the structural system performance of a high-rise building, which is described in detail in other sections, as well as the structural performance of the building after the earthquake, and the grading of the non-structural elements and the time and cost calculations required for the building to serve. Architectural and mechanical components can account for over 70% of

property damage to a building. Loss expenses and down-time costs may exceed the value of the buildings.



Picture 1. This picture is an example of business offices that have prevented the operation after the earthquake. Pictures (a) and (b) show the Sony Kumamoto sensor factory damaged in the earthquake in Japan in April 2016.

2. Methods

Today, there are various design methods and preferences. Such as reinforced concrete buildings, tall structures using steel system and composite (mixed) structures. The rapid construction process and strength of steel, the economical and fire resistance of concrete, and the use of composite structures can solve many problems at the same time, especially in high buildings, play an important role in design preferences.

The buildings in the above mentioned systems are analyzed by advanced analysis methods and the structural system; for example, reinforced concrete shearwalls are designed with elements with perimeter beams and frame systems. Before creating the analysis model of the building, it is explored in detail how to model a reinforced concrete shearwall, beams and columns on the system basis. We can call these as traditional methods and examine them in two groups.

2.1. Design with Traditional Methods

2.1.1. Classic Structural Analysis Method

The engineer pre-calculates, dimensions, and details the structural elements to fulfill the criteria in the regulation. Most of the criteria in the regulation have been developed to provide earthquake performance at some level. However, the targeted performance is often not clear and understandable

2.1.2. Performance-Based Assessment and Design Method

The aim is to provide and control the requirements of the defined performance levels. Performance depends on the amount of damage which the building will take during an earthquake. Some of the regulations used are;

- 1997 - FEMA 273, NEHRP Guidelines for the Seismic Rehabilitation of Buildings
- 2000 - FEMA 356, prestandard and Commentary for the Seismic Rehabilitation of Buildings
- 2007 ASCE / SEI 41-06, 13-17 Seismic Rehabilitation of Existing Buildings
- 2007 Regulation on the building to be constructed in Earthquake Zone Turkey Earthquake 2018
- Building Regulations

Performance based design and assessment of current situation examines the performance levels as Continuous Use, Limited Damage, Controlled Damage and Collapse Prevention as shown in Figure 1 (USRC, 2016).



Figure 1. Performance levels in USRC, 2016.

2.2. Analysis and Design with Next Generation Methods

In recent years, new requirements have brought new solutions in the design process; the performance of the buildings and surroundings during and after the earthquake are taken into account by the different calculation methods and by the grading of the results. The FEMA P58 tool intends to include the non-structural elements in the analysis and to fully simulate a structure and process by interpreting the results with rating programs such as USRC (U.S. Resiliency Council). The structural and non-structural elements are represented by the fragility curves as shown in Figure 2 (FEMA P58, 2002).

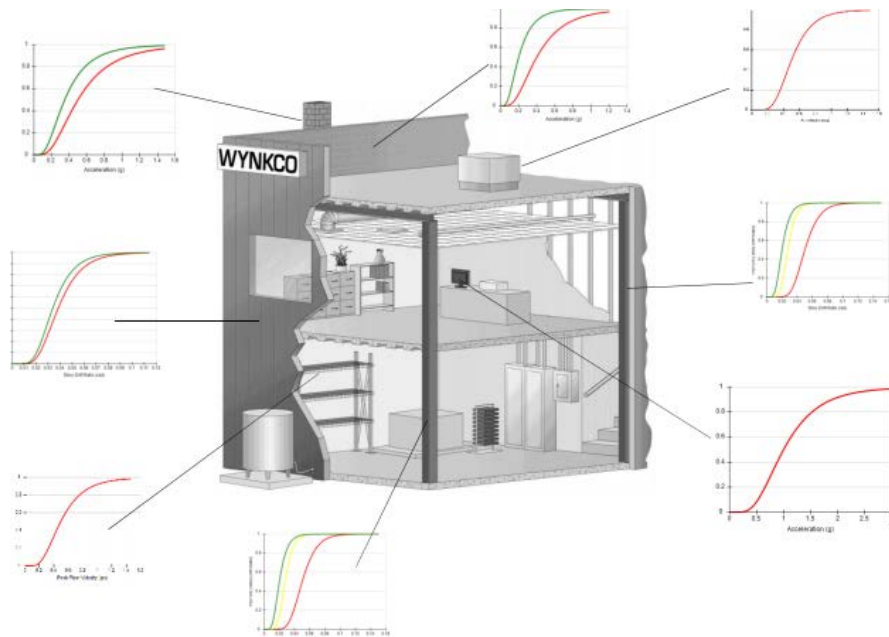


Figure 2. Illustration of fragility curves for the structural and non-structural elements (FEMA P58, 2002).

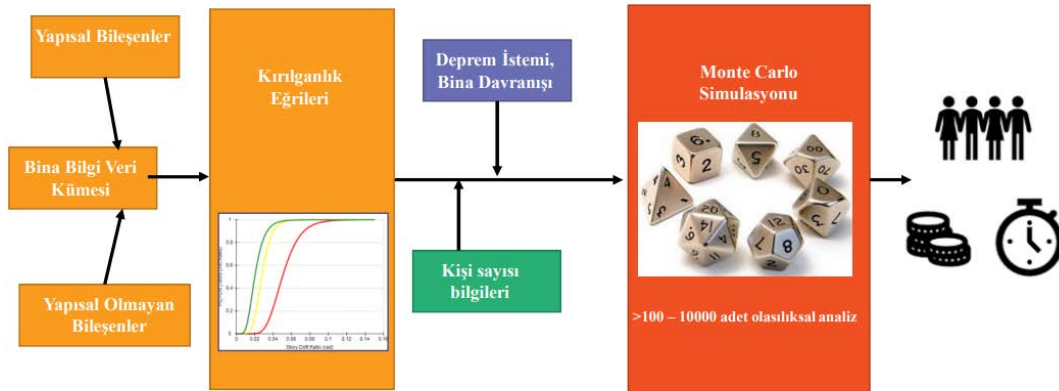


Figure 3. Resilience based analysis flowchart (Emre TOPRAK IMO Seminar 2019)

The flowchart for the resilience based analysis is given in the Figure 3. The analysis steps can be considered as follows:

- The information library is set with the structural and non-structural (cooling towers, generators, shelves) elements information.
- The fragility curves are extracted from FEMA-P58.
- The population density information is required for each floor and per squaremeter.
- Site specific earthquake demand is determined. Performance based structural analysis results such as floor accelerations and drift ratios for each floor are entered as input.
- Monte-Carlo simulation is applied.
- The results are interpreted through the grading systems such as USRC (U.S. Resiliency Council) and REDI (Resilience-based Earthquake Design Initiative).

The probability of repair time and repair cost for a sample building after an earthquake event is shown in the Figure 4. The time required for re-use of the building with a probability of 50% has been calculated as 15 days. The repair cost is calculated based on the data on the structural and non-structural elements for each floor.

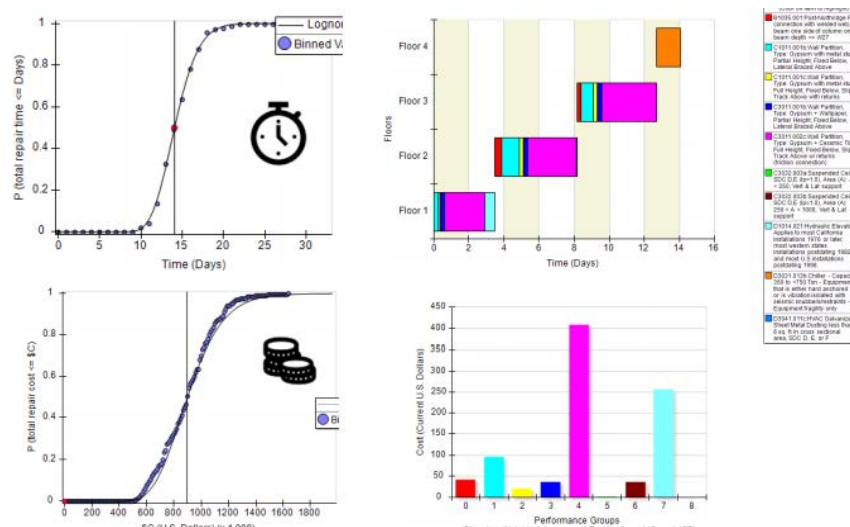


Figure 4. The time-cost graph of a sample building (FEMA P58, 2012).

The Figure 5 shows an example of REDI rating scheme. It is divided into 3 levels as Silver, Gold and Platinum depending on repair time, repair cost and injuries in the analysis results.

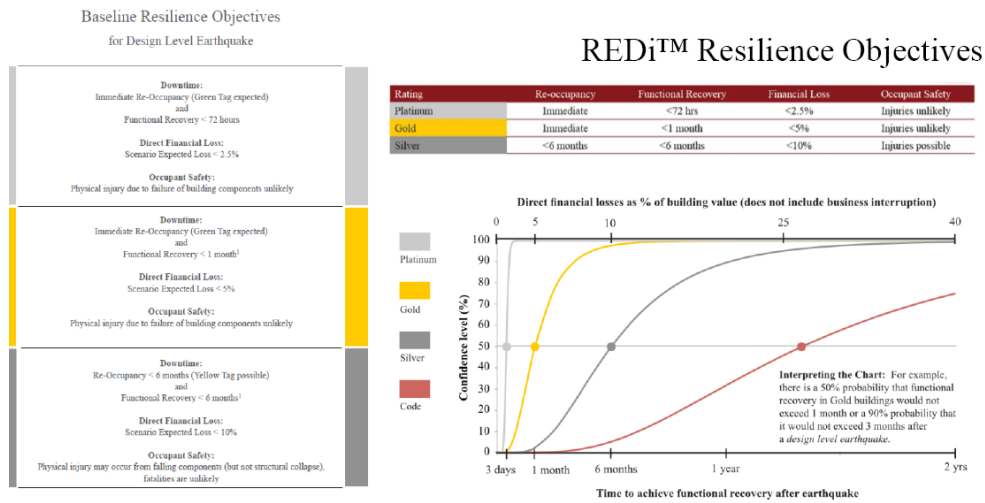


Figure 5. An example of the REDI rating scheme.

3. Modeling, Nonlinear Time History Analysis And Performance Results Of The Structure Used In The Study

3.1. Determining the Properties of the Structure

In this study, a non-linear time history analysis has been carried out for a 28-storey building including ground and roof floors above 2 basement floors. The Figure 6 shows the plan section of the model. The height of the building from the ground is 80.85 meters. Typical floor height is 3.20m on normal floors, 4.00m on ground floor, 3.50m and 3.80m on basement floors.

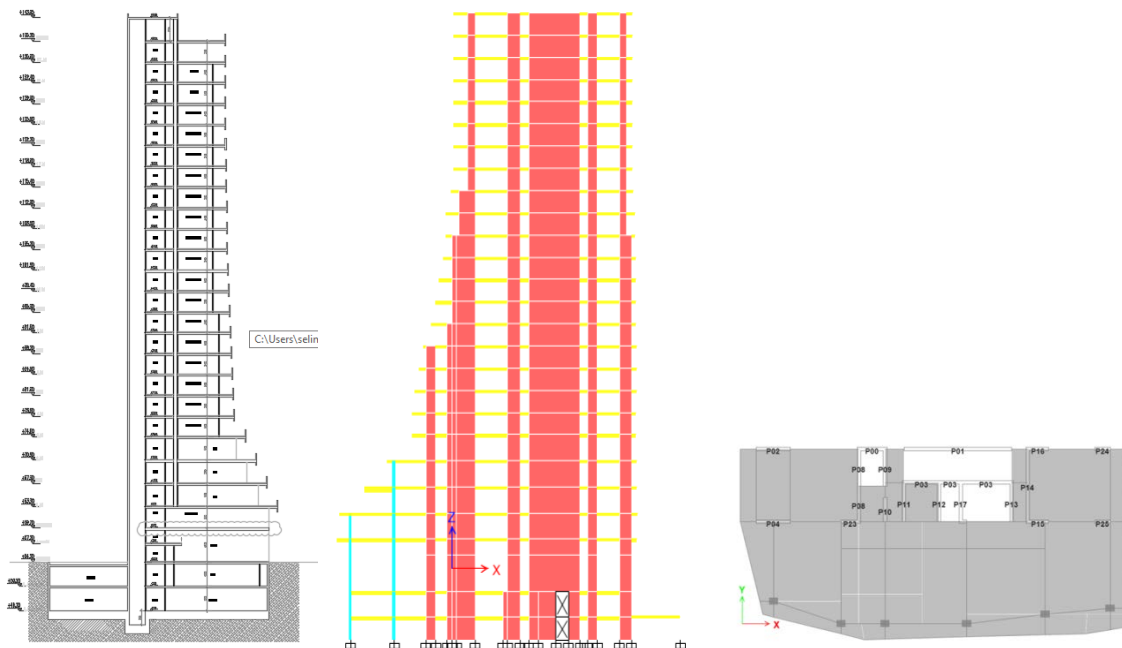


Figure 6. The cross-sectional and plan views of the 28-storey building used in the study

The material properties of the building structure is given in Table 1 and the nonlinear behavior of concrete material (Mander) is shown in Figure 7.

Material Properties Used in Design:

Table 1. Mechanical properties of concrete and reinforcing steel materials used in the analysis model

	Expected Resistance
characteristic fck Resistance (kN / m2) C40	52000
Modules of Elasticity Ec (Mander et al., 1988) (kN / m2)	36.056.000
Elasticity Module Ec (TS-EN 1992-1) (kN / m2)	36.076.000
Shear Modulus G (kN / m2)	15.032.000
Heavy Unit Volume. γbeto kN / m3	25
Poisson's ratio ν ν -	0.2
γmc -	1.5
Reinforcement (B420-C) (kN / m2)	504.000
Modulus of elasticity (ES)	200.000.000

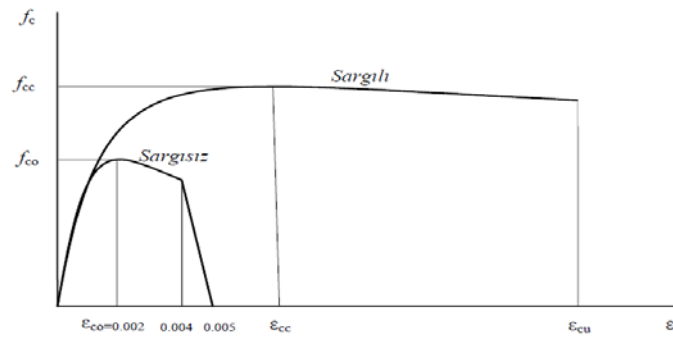


Figure 7. Coil winding concrete stress and strain relations

Effective Section Stiffness values; In the nonlinear analysis model, the effective cross-section stiffnesses are automatically calculated from the material behavior curves in the elements included in the model according to the spread plasticity approach. Effective section stiffnesses for columns and beams modeled using bar elements according to the stacked plasticity approach are calculated using the following correlation according to TBDY2018 Section 5.4.5.

$$(EI)_e = \frac{M_y L_s}{\theta_y} \frac{L_s}{3} \quad \theta_y = \frac{\phi_y L_s}{3} + 0.0015 \left(1 + 1.5 \frac{h}{L_s} \right) + \frac{\phi_y d_b f_{ye}}{8 \sqrt{f_{ce}}}$$

It is the yield moment calculated by considering the axial load effect at the ends of the beams and columns M_y in this relation. Plastic hinge θ_y flow rotation for sections is calculated from the relation above.

The figure 8 (a) shows the Perform 3D model which is the nonlinear calculation tool, and (b) shows the preliminary design model in Etabs 2017. The Figure 8 (c) shows the plan view of the model.

The results presented in this study are based on the preliminary design of the CSI ETABS analysis model and the CSI Perform3D program for nonlinear time history analysis of the building.

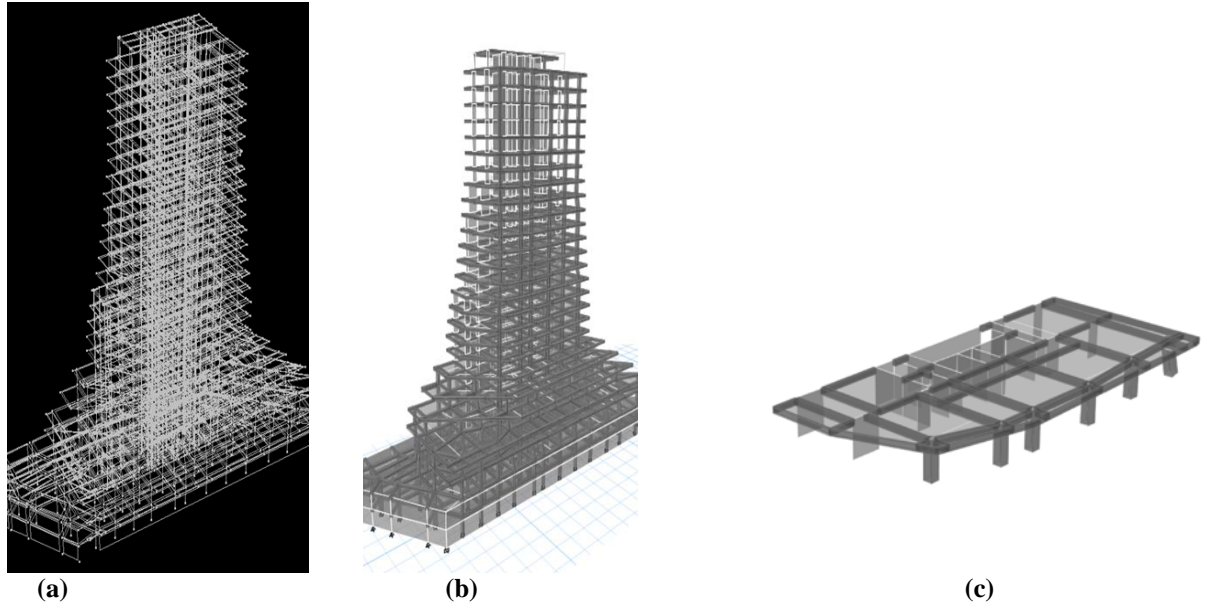


Figure 8. This figure is the Perform 3D analytical model (a), Etabs 2017 model (b), the plan view of the Perform3D analysis model (c).

The figure 9 and figure 10 preliminary design parameters used in the calculations are determined by TBDY 2018 in the following section.

Bina Kullanım Sınıfı	Binanın Kullanım Amacı	Bina Önem Katsayısı (I)
BKS = 1	Deprem sonrası kullanımı gereken binalar, insanların uzun süreli ve yoğun olarak bulunduğu binalar, değerli eşyanın saklandığı binalar ve tehlikeli madde içeren binalar a) Deprem sonrasında beman kullanılması gerekli binalar (Hastaneler, dispenseler, sağlık ocakları, itfaiye bina ve tesisleri, PTI ve diğer haberleşme tesisleri, ulaşım istasyonları ve terminalleri, enerji üretim ve dağıtım tesisleri, vilayet, kaymakamlık ve belediye yönetim binaları, ilk yardım ve afet planlama istasyonları) b) Okullar, diğer eğitim bina ve tesisleri, yurt ve yatakhaneler, askeri kırsallar, cezaevleri, vb. c) Müzeler d) Toksik, patlayıcı, parlayıcı, vb. özellikleri olan maddelerin bulunduğu veya depolandığı binalar	1.5
BKS = 2	İnsanların kısa süreli ve yoğun olarak bulunduğu binalar Ahiyeri merkezleri, spor tesisleri, sinema, tiyatro, konser salonları, ibadethaneler, vb.	1.2
BKS = 3	Diğer binalar BKS-1 ve BKS-2 için verilen tanımlara girmeyen diğer binalar (Konutlar, işyerleri, oteller, bina türü enlütürü yapıları, vb.)	1.0

DD-2 Deprem Yer Hareketi Düzeyinde Kısa Periyot Tasarım Spektral İvme Katsayısı (S_{DS})	Bina Kullanım Sınıfı	
	BKS = 1	BKS = 2, 3
$S_{DS} < 0.33$	DTS = 4a	DTS = 4
$0.33 \leq S_{DS} < 0.50$	DTS = 3a	DTS = 3
$0.50 \leq S_{DS} < 0.75$	DTS = 2a	DTS = 2
$0.75 \leq S_{DS}$	DTS = 1a	DTS = 1

Figure 9. Building use class (a) TBDY 2018 Table 3.1 and Earthquake design class (b)

Bina Yükseklik Sınıfı	Bina Yükseklik Sınıfları ve Deprem Tasarım Sınıflarına Göre Tanımlanan Bina Yükseklik Aralıkları [m]		
	DTS = 1, 1a, 2, 2a	DTS = 3, 3a	DTS = 4, 4a
BYS = 1	$H_N > 70$	$H_N > 91$	$H_N > 105$
BYS = 2	$56 < H_N \leq 70$	$70 < H_N \leq 91$	$91 < H_N \leq 105$
BYS = 3	$42 < H_N \leq 56$	$56 < H_N \leq 70$	$56 < H_N \leq 91$
BYS = 4	$28 < H_N \leq 42$	$42 < H_N \leq 56$	
BYS = 5	$17.5 < H_N \leq 28$	$28 < H_N \leq 42$	
BYS = 6	$10.5 < H_N \leq 17.5$	$17.5 < H_N \leq 28$	
BYS = 7	$7 < H_N \leq 10.5$	$10.5 < H_N \leq 17.5$	
BYS = 8	$H_N \leq 7$	$H_N \leq 10.5$	

Binanın Kullanım Amacı	n
Depo, antrepo, vb.	0.80
Okul, öğrenci yurdu, spor tesisi, sinema, tiyatro, konser salonu, ibadethane, lokanta, mağaza, vb.	0.60
Konut, işyeri, otel, hastane, otopark, vb.	0.30

Figure 10. Building height class (a) TBDY 2018 Table 3.1 and Live load participation coefficient 3.1

3.2. Design Earthquake Levels

The design earthquake levels have been taken from the Turkish Building Earthquake Regulation (Türkiye Bina Deprem Yönetmeliği, TBDY 2018).

3.2.1. Earthquake Level for DD1

This earthquake level refers to the most severe earthquake ground movements that buildings can be exposed to. The probability of the earthquake at dd1 level to exceed 50 years is 2%, the corresponding return period is 2475 years

3.2.2 Earthquake Level for DD2

This level of earthquake refers to sparse but severe earthquake ground movements that are not very likely to occur during the service life of buildings. The probability of a D2 level earthquake to exceed 50 years is 10%, the corresponding return period is 475 years.

3.2.3. Earthquake Level for DD3

This level of earthquake refers to earthquake ground movements that are likely to occur during the service life of the buildings, relatively frequent but not very high severity. The probability of the DD3 level earthquake to overcome in 50 years is 50%, and the corresponding return period is 72 years.

3.2.4. Earthquake Level for DD4

This level of earthquake refers to earthquake ground movements that are likely to occur during the service life of the buildings, relatively frequent but not very high severity. The probability of the DD4 level earthquake to overcome in 50 years is 68% and the corresponding return period is 43 years

3.3. Scaled Motion to be used in the analysis

A site-specific earthquake hazard study has been carried out to be used for nonlinear time history analysis of the building. Scaled records for DD1 earthquake level are as follows, rsn4841_chuets-o in Japan, rsn4843_chuets-o in Japan, rsn4872_chuets-o in Japan, rsn5478_iwat Japan, rsn5623_iwat Japan, rsn5775_iwat Japan, rsn6891_darfield NewZealand, rsn1633_manjil Iran, rsn1787_hectorm, rsn750_lomapiet, rsn751_lomapiet records are used. (Records were obtained from PEER website <https://ngawest2.berkeley.edu/sites>).

For the nonlinear analysis, site-specific earthquake records are scaled as shown in the figure 11.

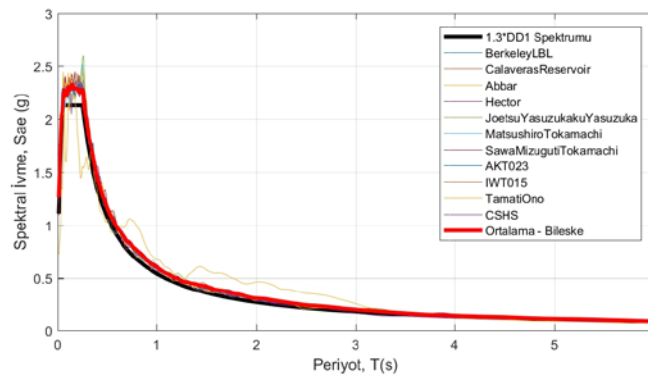


Figure 11. The SRSS of the records acceleration spectra scaled for DD1 earthquake level

3.4. Nonlinear Time History Analysis Results

Floor relative displacement readings have been made from 4 different points on each floor as shown in the Figure 12. The floor drift ratio limit has been assigned as (3%) for the DD1 earthquake level and for the collapse prevention (GÖ) performance level according to the TBDY 2018 as shown in the Table 2.

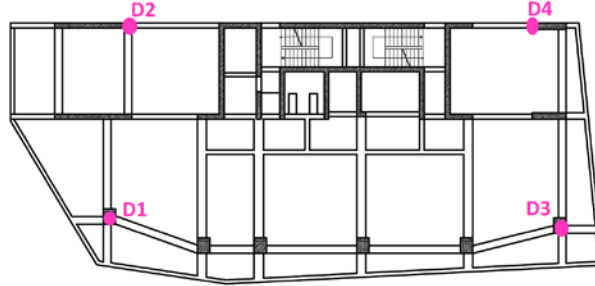


Figure 12. This figure shows the points where the results of relative floor displacements are read.

Table 2. This table shows the limit values given for relative floor displacements in TBDY 2018.

Earthquake Level	DD1
Target Performance	Collapse Prevention
Drift ratio limit	3.0% (Mean)

The relative floor displacement has been checked for each point in both directions as shown in the Figure 13. The limit values in the regulation are shown with a dashed line. The lines drawn in dark color represent the average value of the results of 11 earthquakes.

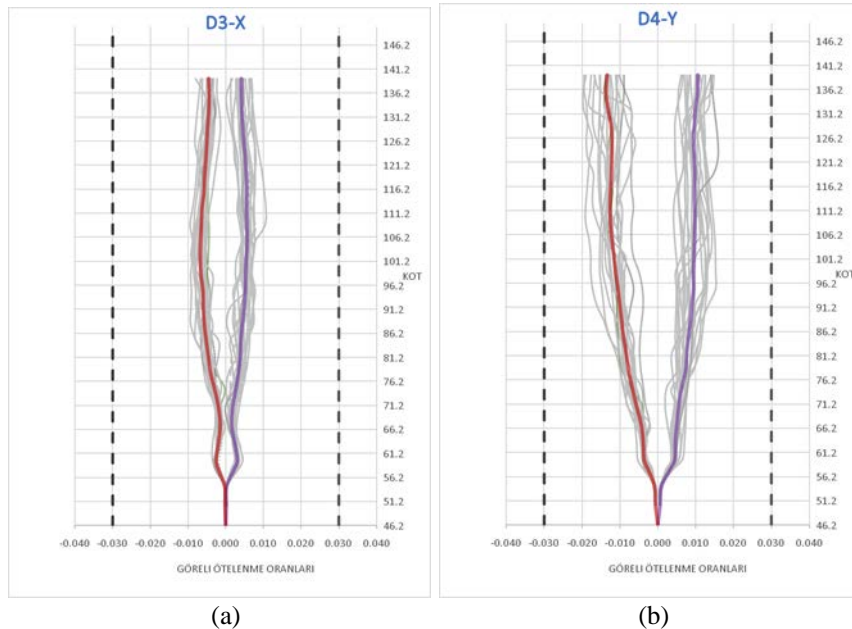


Figure 13. The relative floor displacements in the X direction (a), the relative floor displacements in the Y direction (b).

In the deformation control for shear walls, unit deformation controls were performed for all shear walls using the measurement elements (straingauges) as shown in the Figure 14. The readings for the shearwalls

from the analysis results are shown in the Table 3. The strain levels for the concrete and reinforcing steel for the Collapse Prevention and Controlled Damage performance levels according to the TBDY 2018 are shown in the Table 4. As it has been seen that the analysis result readings are well below the upper limits defined by the TBDY 2018.

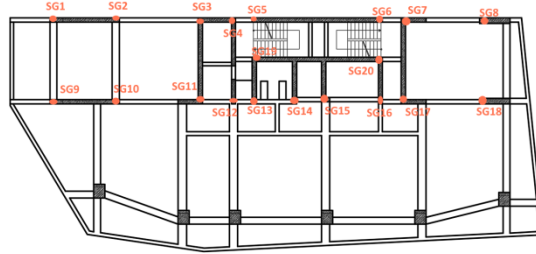


Figure 14. The location of the strain gauges placed on the shearwall in the model

Table 3. In this table, the unit strain values read at the ends of the system walls are given

Shearwall IDs	ϵ_c (GO)	Shearwall IDs	ϵ_c (GO)
P00	0.009618	P13	0.009257
P01	0.007155	P14	0.007875
P02	0.008438	P15	0.009618
P03	0.006909	P16	0.009618
P04	0.008438	P17	0.009257
P08	0.007875	P18	0.009618
P09	0.009257	P22	0.009618
P10	0.009618	P23	0.009618
P11	0.009257	P24	0.009746
P12	0.009257		

Table 4. The upper strain limits according to various cross-section damage limits (TBDY, 2018)

Earthquake Level;		
DD1 Target Performance	Collapse Prevention	Controlled Damage
Confined concrete pressure unit deformation limit (ϵ_{cg})	$0.004 + 0.0035 * \sqrt{(\omega_w A)} \leq 0,0180$	$0.75 * \epsilon_{cg0}$
Reinforcement unit deformation limit (ϵ_s)	0,032	0,024

Here; ω_w shows the active hoop ratio.

Shearwalls Shear Capacity Control

The control of the shear capacities for the shear walls in the building has been made for the shear forces occurring at the DD1 earthquake level for all shear walls. According to the results as shown in the Figure 15, the shear force values on the shearwalls are below the limit value ($V_e \leq 0.85A_{ch} * \sqrt{f_{ck}}$) red dashed line.

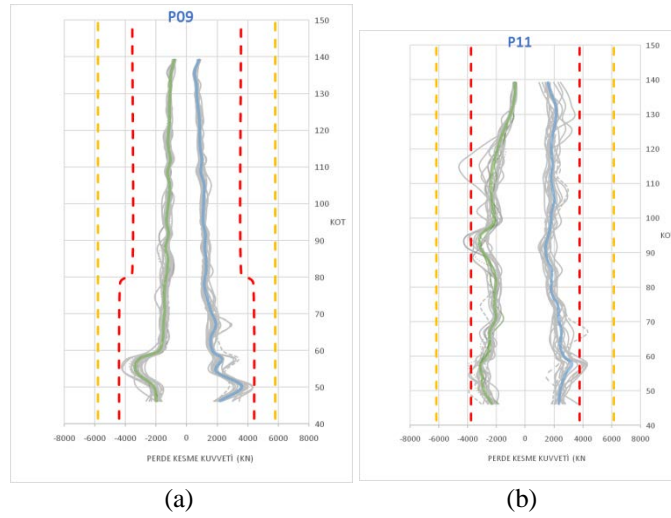


Figure 15. The shear force values received by the shearwall P09 (a) and shearwall P11 (b)

Columns Plastic Rotation Control

Plastic hinge rotations at the end regions of column elements of the nonlinear model have been checked. Column plastic rotations do not exceed the Performance Level Controlled Damage (KH) upper limits as shown in the Figure 16.

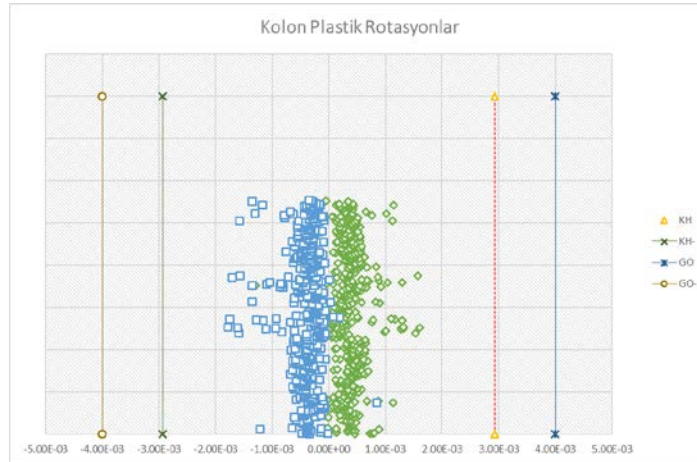


Figure 16. Comparison of Column Rotations with Plastic Rotational Capacities

According to above results in the light of DD1 earthquake effects, the following evaluations have been reached for the nonlinear performance analysis;

- Relative floor displacements in the structure provide the Collapse Prevention level.
- The strain levels occurring in the shearwalls of the building are below the allowable limit values.
- The shear strength of the shearwalls in the building is sufficient
- The deformation demands that occur in the columns and beams in the building are below the limits allowed by the regulation.
- Tie beams in the structure provide the Collapse Prevention level.

4. Performance Based Design of 28 Story Residential Building Using Time Based Assessment Approach of FEMA-P58 and Its Pact Tool

This chapter provides an example application of the time-based performance for 28 story RC residential building for assessment methodology using nonlinear response history analysis in the Performance Assessment Calculation Tool (PACT) with provided fragility and consequence function data. The work necessary to obtain a probable maximum loss value that reflects the repair cost, expressed as percentage of building replacement cost, having a 10% probability of exceedance over a 50-year loan period for an office building is presented here as follows.

- Obtain site and building description,
- Select assessment type and performance measure,
- Assemble building performance model,
- Select analysis method and construct analytical building model,
- Define earthquake hazards,
- Analyse building response,
- Input response data and calculate performance
- Review results for selected performance measures,

Select assessment type and performance measure

Time-based assessment will be performed with building performance expressed in terms of average annual repair cost in dollars. The resulting cost distribution is used to determine the loss associated with a 10% probability of exceedance over a 50-year period of time and converted from dollars to percentage of replacement cost.

Assemble building performance model

The building performance model has been constructed in PACT by following the sequence: providing project information, building characteristics selecting fragility specifications and performance groups, identifying collapse fragility and collapse modes, and providing residual drift fragility. The building informations input are as follows (see. Figure 15 (a) and 15 (b), in which PACT input)

- Number of floors: 28
- Total building cost: \$ 9,548,955 were estimated to be.
- Replacement Time: Estimated as 576 days.
- Core and Shell Replacement Cost: Estimated as \$ 3,342,135.
- Maximum Workers per Square Foot: Default value of 0.001 is used.
- Total Loss Threshold (as Ratio of Total Replacement Cost): Default value of 1.0 is used.
- Floor Area: 860.95 m²
- Floor Height: 3.4m Variation in floor height is input via the Floor Number drop down selector, which also permits input of non-typical floor areas.

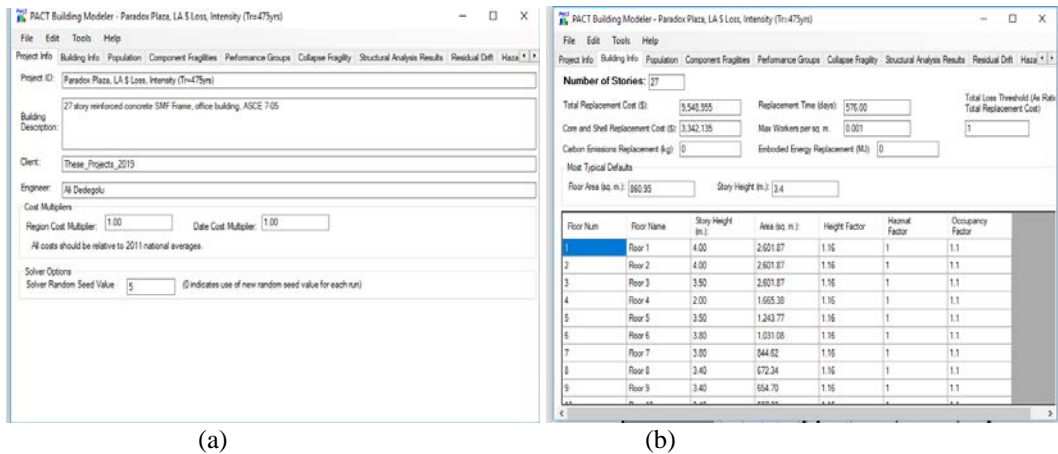


Figure 17. In this way, the PACT project in (a) and PACT building data entry screens (b)

FEMA P58 -PACT according to the type of structure is necessary to introduce the people of the time-dependent density daily chart of the building. In this study, we use the figure because it is the type of building housing figure 18 'as seen in the graph human density is high, the hours of the day and low at night.

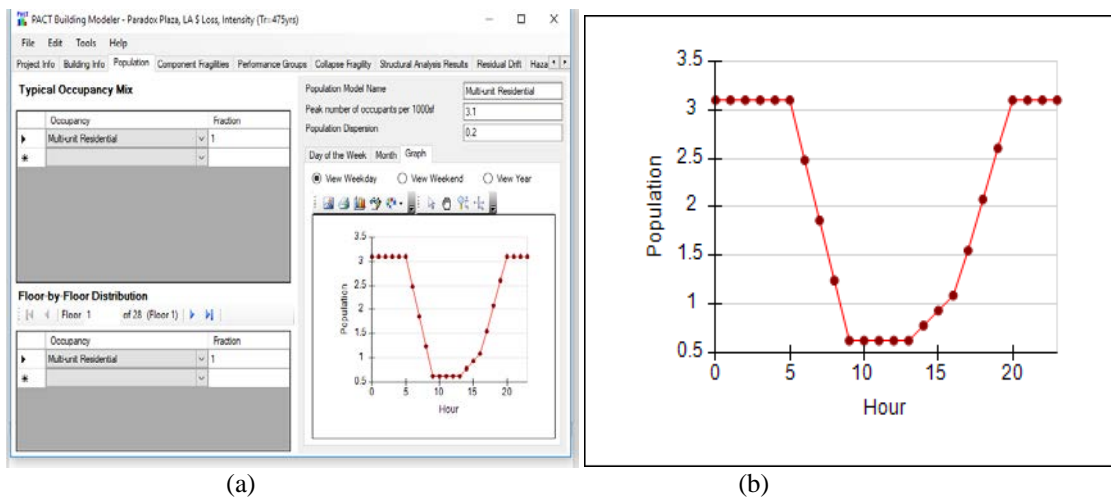


Figure 18. Building on the identification of people have busy times and density chart

4.1. Structural Components

As structural components, columns, beams, shear wall and slabs in the building are mentioned

4.1.1. Structural Component Fragility Specifications

Structural components are input based on the basic building characteristics previously described. To input structural fragility groups, the dropdown menu of selections in the Component Fragilities tab, shown in Figure 19 are utilized. The following information summarizes the structural components included in the performance assessment model.

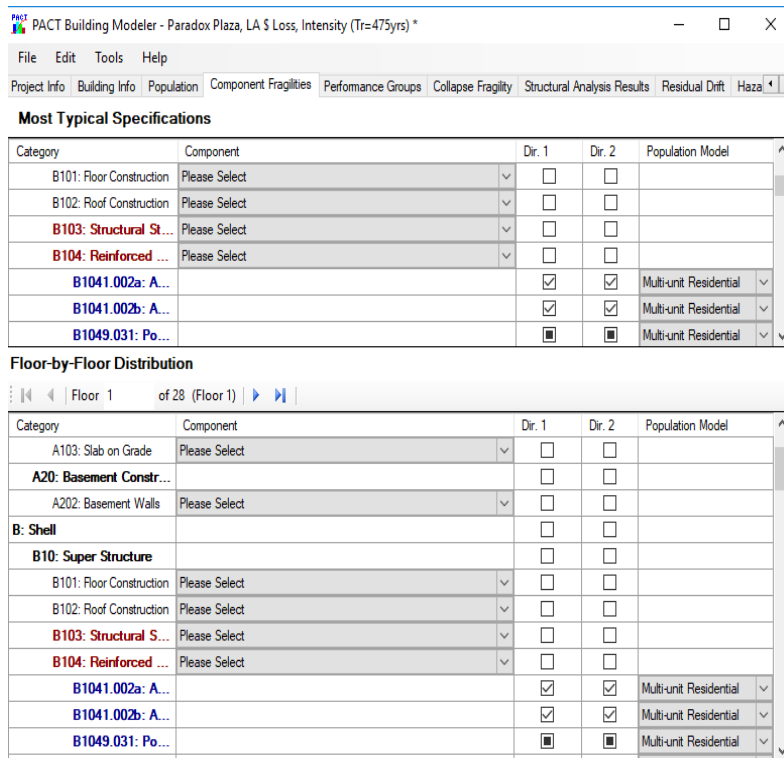


Figure 19. Beam-Column joints fragility curve definition

4.1.2. Structural Component Performance Groups

For each floor, the number of special moment frame beam-column joints vulnerable to story drift in each building direction are entered for each of the pre-selected specifications. Figure 20 summarize the defining performance groups in PACT with A, B, C, D, E-the building axes in X (2) direction and 1, 2, 3, 4, 5, 6, 7-in Y (1) direction. Input of the post-tensioned slab/column joint information is similarly inserted at each floor; however, these fragilities are input as non-directional. There are for example 77, joints for floor 1.

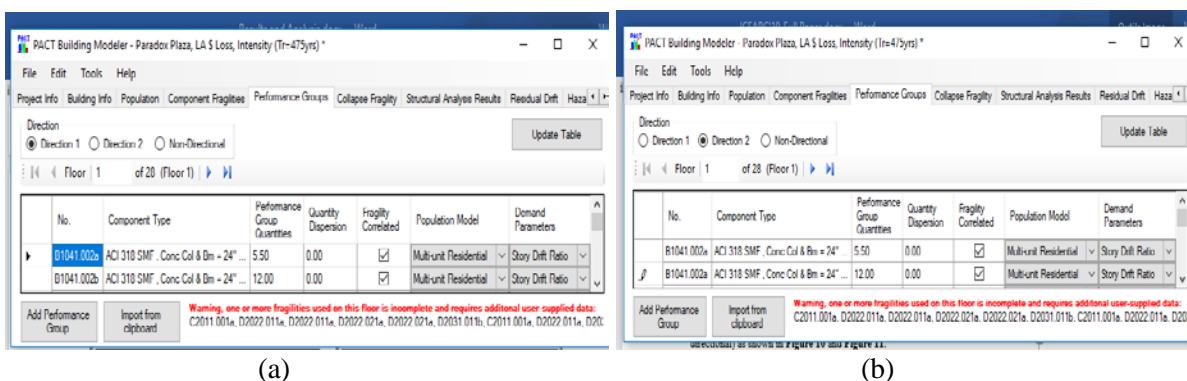


Figure 20. The performance group definition process is repeated for each floor and for each direction (including non-directional) as shown in Floor 1

4.2. Non-Structural Components

The process of identifying and selecting the type and distribution of the nonstructural components can be greatly simplified by the use of the Normative Quantity Estimation Tool, provided in Volume 3 of PACT. This tool can be used to generate a floor-by-floor listing of nonstructural components with

estimates of their performance group quantities with the simple input of building floor areas and occupancies as shown in figure 19

- Water Tank, Water Tank 15 M³ Module. Hsu = 1.5m. As Steel Tank + Water = 1800kg / m² (30cm Floating Concrete Qaeda Qaeda Excluded)
- Vrv Air Conditioning Outdoor Unit Cooling Devices (except for H = 30cm Steel Qaeda Qaeda) = 350kg / m² (excluding Qaeda)
- Cooling Chiller Unit (except for 4-Qaeda Corner Wedge H = 50cm concrete Qaeda Qaeda) = 550kg / m² (excluding Qaeda)
- Ventilation Equipment Plant = 250-350 Kg / M² (Excluding Mount)
- HRV (Heat Recovery Devices Cabinet Type) De Floor Office Tower Some of the Subject is = 250 kg / m² (excluding Qaeda)
- Boiler (Floor Standing Condensing) = 200-450 Kg / M² (Excluding Mount)
- Stairs, elevator pressurization And Smoke Exhaust Fans = 210kg / 0,42m² = 500kg / m² (Atrium Steel Roof Fans Smoke necessarily be reported to the main Static Group)
- Cell Exhaust fans (kitchen wc..vs) = 150 to 250 kg / m²
- Or Norm Cooling Heating Pumps = 1.010kg / 0,98m² = 1030kg / m²
- Horizontal Equilibrium Tank (Large System in) = 500-750kg / m² (Varies by this system size)
- Expansion Tanks = 1000-2000kg / M²
- Cooling Tower Equipment = 34.000kg / 35m² = 971kg / M²
- I 2.Bod Energy Room Floor
- Server Computing 3.Normal Room Floor
- Facade elements and Glass Facades in -All
- Front Purifier Attic -7 Ton

OCCUPANCY		Fragility Number	Fragility Name	Assumed Quantity per component	Quantity	
Type	Occupancy #				Directional	Non Directional
APARTMENT	1	B2022.001	B2022.001 Curtain Walls - Generic Midrise Stick-Bu	30 SF	25.58	--
APARTMENT	1	B3011.011	B3011.011 Concrete tile roof, tiles secured and com	100 SF	--	16.37
APARTMENT	1	C1011.001a	C1011.001a Wall Partition, Type: Gypsum with meta	100 LF	6.14	--
APARTMENT	1	C3011.001a	C3011.001a Wall Partition, Type: Gypsum + Wallpap	100 LF	1.95	--
APARTMENT	1	D2021.011a	D2021.011a Cold Water Piping (dia > 2.5 inches), SQ	1000 LF	--	0.08
APARTMENT	1	D2022.011a	D2022.011a Hot Water Piping - Small Diameter Thr	1000 LF	--	1.08
APARTMENT	1	D2022.021a	D2022.021a Hot Water Piping - Large Diameter Wel	1000 LF	--	0.15
APARTMENT	1	D2031.011b	D2031.011b Sanitary Waste Piping - Cast Iron w/fin	1000 LF	--	0.62
APARTMENT	1	D3041.011a	D3041.011a HVAC Galvanized Sheet Metal Ducting	1000 LF	--	0.26
APARTMENT	1	D3041.031a	D3041.031a HVAC Drops / Diffusers in suspended c	10 EA	--	4.09
APARTMENT	1	D3041.041a	D3041.041a Variable Air Volume (VAV) box with in-	10 EA	--	2.05
APARTMENT	1	D2022.011a	D2022.011a Hot Water Piping - Small Diameter Thr	1000 LF	--	0.03
APARTMENT	1	D2022.021a	D2022.021a Hot Water Piping - Large Diameter Wel	1000 LF	--	0.03
APARTMENT	1	D4011.021a	D4011.021a Fire Sprinkler Water Piping - Horizonta	1000 LF	--	1.13
APARTMENT	1	D4011.031a	D4011.031a Fire Sprinkler Drop Standard Threaded	100 EA	--	0.61
APARTMENT	1	B2022.001	B2022.001 Curtain Walls - Generic Midrise Stick-Bu	30 SF	25.58	--
APARTMENT	1	B3011.011	B3011.011 Concrete tile roof, tiles secured and com	100 SF	--	16.37
APARTMENT	1	C1011.001a	C1011.001a Wall Partition, Type: Gypsum with meta	100 LF	6.14	--
APARTMENT	1	C3011.001a	C3011.001a Wall Partition, Type: Gypsum + Wallpap	100 LF	1.95	--

Figure 21. In this way, PACT program introduction of non-structural elements

4.3. Define earthquake hazards

For time-based assessments, nonlinear response history analyses are conducted for m sets of n ground motion pairs each, scaled to appropriate intensity values using the procedures of volume 1, Chapter 4 of FEMA P58. a value of 8 is recommended for m . For very weak buildings, M can be taken smaller than 8. For buildings with high resistance, it may be necessary to increase the number of segments or increase the range of segments to obtain stable results.

Ground motion records for time-based assessments are generated as follows:

step 1. Determine the building's fundamental translational periods in two orthogonal directions. (T_1^X and T_1^Y).

building period in both the vertical directions are ; $T_1^X = 2.94\text{sec}$ $T_1^Y = 4.06\text{sec}$

step 2. Then, the average fundamental period of the building is $\bar{T} = \frac{T_x + T_y}{2} = 3.5\text{sec}$

step 3. Obtain a seismic hazard curve for $S_a(\bar{T})$

Although site-specific seismic hazard analysis can be used, for this example, the Java Ground Motion Calculator, available for download from "Türkiye Deprem Tehlike Haritaları" İnteraktif Web App. at tdth.afad.gov.tr is used, as previously illustrated in Figure 20.

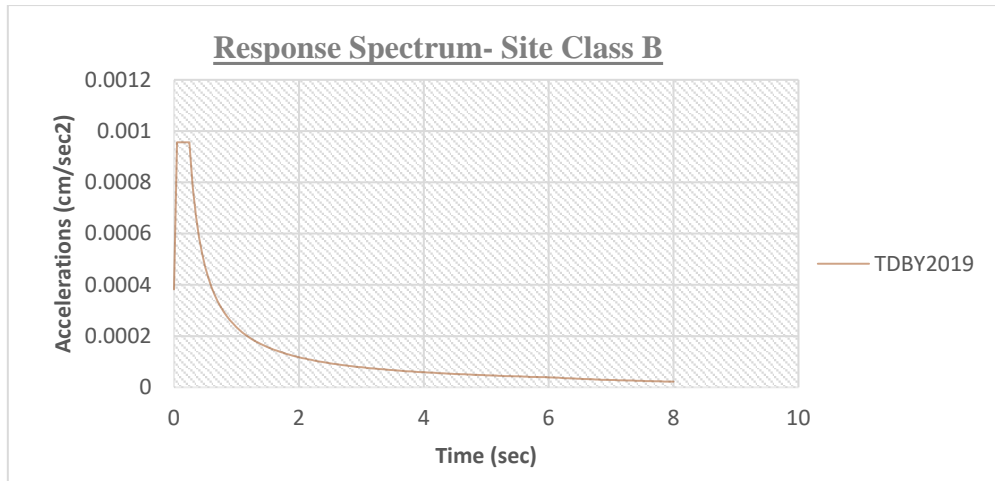


Figure 22. Seismic hazard curve, Site Class ZB, level DD2

Step 4. Define $S_a^{min}(T)$ and $S_a^{max}(T)$ that span between building response that produces negligible damage to response that produces significant probability of collapse. For $\bar{T} = 3.5\text{sec}$ $S_a^{min}(T)$ be taken as;

$$S_a^{min}(T) = \frac{0.05}{\bar{T}} = \frac{0.05}{3.5} = 0.014g$$

$$S_a^{max}(T) = 2 * S_a(\bar{T})$$

$S_a(\bar{T})$ value is interpreted as 0.938g.

$$S_a^{max}(T) = 2 * 0.938 = 1.876g$$

Step 5. Divide the seismic hazard curve into 8 segments that span the range of $\hat{S}(T)$ from $S_a^{min}(T)$ to $S_a^{max}(T)$.

(($S_a^{min}(T)$ to $S_a^{max}(T) = \hat{S}(T)$, $S_a^{max}(T) = 1.876g > \hat{S}(T) = 1.56g$ büyük olduğu için $1.56g$ alınmıştır

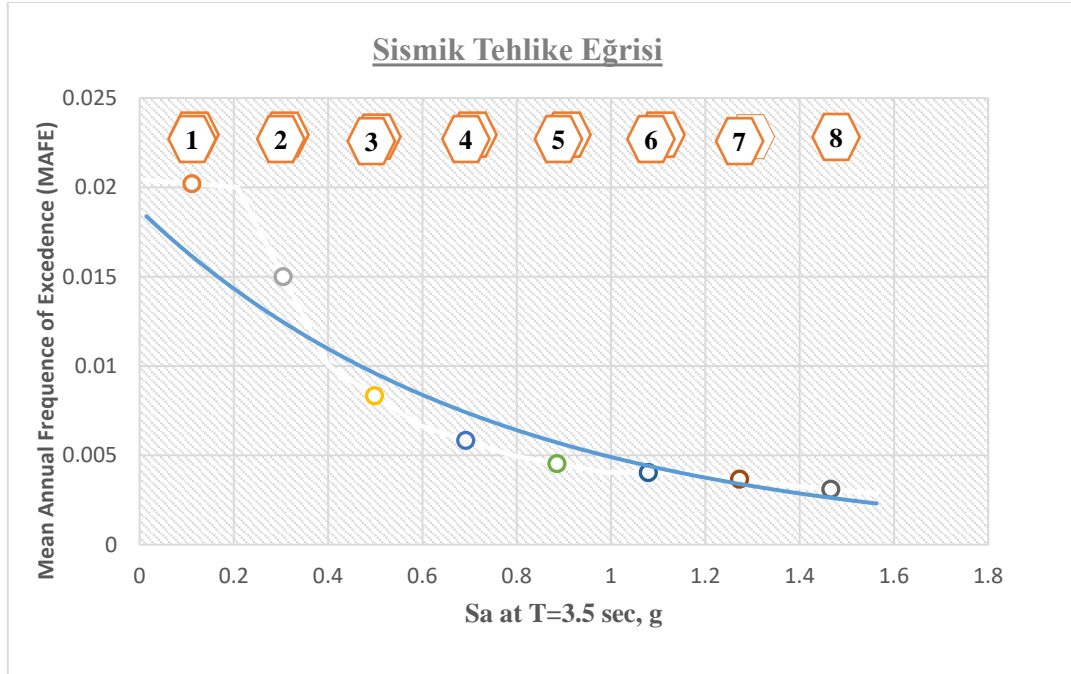


Figure 23. Illustrates the striping of the seismic hazard curve of Figure 5-2 producing 8 equal S_a -width segments spanning the range of $\hat{S}(T)$ from $0.014g$ to $1.876g$ (($S_a^{min}(T)$ to $S_a^{max}(T) = \hat{S}(T)$, because to $S_a^{max}(T) = 1.876g > \hat{S}(T) = 1.56g$). Each segment has a width

Step 6. The central value of $\hat{S}(T)$ at the midpoint of each segment is determined together with its mean annual frequency of exceedance. Table 5-3 summarizes these data.

Table 5. Intensity Segment Values

Spectral Segments	PGA = S (T)	Frequency Values
1	0.11109	0.020205
2	0.30469	0.015
3	0.49829	0.008335
4	0.69189	0.005835
5	0.88549	0.00453
6	1.07909	0.00403
7	1.2727	0.003665
8	1.4663	0.003095

4.4. Select analysis method and construct analytical building model

The structure is analysed using nonlinear response history analysis. A three-dimensional analytical model is assembled as described in Section 3.2.2 and Volume 1, Chapter 5 of FEMAP58. We have used ETAB2017 and PERFORM3D for this purpose.

Table 6. Summary of Structural Analysis Results (drift and acceleration values according to floors, It is taken from nonlinear analysis Perform 3D).

Intensity 5 Sa(T)=0.885g			Intensity 6 Sa(T)=1.079g			Intensity 7 Sa(T)=1.273g			Intensity 8 Sa(T)=1.466g		
Demand	Median		Demand	Median		Demand	Median		Demand	Median	
KAT	Δ_i	a_i	KAT	Δ_i	a_i	KAT	Δ_i	a_i	KAT	Δ_i	a_i
13	0.00719	1.56555	13	0.00446	1.38828	13	0.00212	0.66847	13	0.00361	0.66693
22	0.00731	1.65939	22	0.00453	1.48368	22	0.00216	0.73422	22	0.00367	0.725
21	0.00733	1.7244	21	0.00454	1.5331	21	0.00216	0.74463	21	0.00368	0.74047
20	0.00735	1.77005	20	0.00455	1.57291	20	0.00217	0.76271	20	0.00369	0.75892
19	0.00723	1.60287	19	0.00448	1.43561	19	0.00213	0.71441	19	0.00363	0.70397
18	0.00694	1.70137	18	0.0043	1.51246	18	0.00205	0.73435	18	0.00348	0.73034
17	0.0067	1.85437	17	0.00415	1.64713	17	0.00197	0.79756	17	0.00336	0.79403
16	0.00663	1.66341	16	0.00411	1.48799	16	0.00196	0.7375	16	0.00333	0.72781
15	0.00644	1.67112	15	0.00399	1.49248	15	0.0019	0.73585	15	0.00323	0.72761
14	0.00617	1.72881	14	0.00382	1.54353	14	0.00182	0.76027	14	0.0031	0.75204
13	0.0054	1.59088	13	0.00335	1.42549	13	0.00159	0.71037	13	0.00271	0.69962
12	0.00527	1.75156	12	0.00326	1.57624	12	0.00155	0.79639	12	0.00264	0.78034
11	0.00538	1.79612	11	0.00333	1.61048	11	0.00159	0.80431	11	0.0027	0.79149
10	0.00527	1.64913	10	0.00327	1.47843	10	0.00155	0.73796	10	0.00264	0.72635
9	0.00475	1.74398	9	0.00294	1.55473	9	0.0014	0.76198	9	0.00238	0.75515
8	0.00473	1.76198	8	0.00293	1.57577	8	0.00139	0.78038	8	0.00237	0.77037
7	0.00486	1.99141	7	0.00301	1.77566	7	0.00143	0.87085	7	0.00244	0.86282
6	0.00468	1.57048	6	0.0029	1.40091	6	0.00138	0.68798	6	0.00235	0.68129
5	0.00494	1.44163	5	0.00306	1.28344	5	0.00146	0.62622	5	0.00248	0.62165
4	0.00467	1.71101	4	0.00289	1.53291	4	0.00138	0.76354	4	0.00234	0.75212
3	0.00447	1.35813	3	0.00277	1.21107	3	0.00132	0.59407	3	0.00224	0.58855
2	0.00437	1.78219	2	0.00271	1.5992	2	0.00129	0.80063	2	0.00219	0.78716
1	0.00424	1.70107	1	0.00262	1.51769	1	0.00125	0.74579	1	0.00213	0.73837
-4	0.00378	1.29132	-4	0.00234	1.1397	-4	0.00111	0.54	-4	0.0019	0.54209
-2	0.00351	1.63069	-2	0.00218	1.44714	-2	0.00104	0.6986	-2	0.00176	0.69631
-3	0.00236	1.89171	-3	0.00146	1.68264	-3	0.0007	0.81857	-3	0.00118	0.81351
-1	0.0005	1.17383	-1	0.00031	1.04576	-1	0.00015	0.51142	-1	0.00025	0.50725

4.5. Input Response Data and Calculate Performance

Structural analysis results for each of the 8 intensity levels are input to PACT on the Structural Analysis Results tab. Figure 25 illustrates the drift input values for intensity 4, direction 1. Input includes spectral acceleration ($S_a = 0.692g$), dispersion ($\beta_m = 0.47$) and includes input for all 7 demand vectors.

5. Evaluation

PACT displays assessment results on the Time-Based Results tab as shown in Figure 2, which shows annual probability of exceedance for repair cost of different amounts as well as average annual loss values. In the illustration, the average annual probability of collapse is shown in the box at the upper left-hand corner of the figure as 0.0006475. This is equal to a mean return period for collapse of $\frac{1}{0.0006475} = 1544$ years. Similarly, the box below this indicates an average annual probability of 0.012 for damage being so severe that an unsafe placard is posted on the building, equal to a mean return period of approximately 85 years. To determine the repair cost that has a 10% probability of non-exceedance over the 50-year loan period, it is necessary to calculate the corresponding return period for such a loss. The mean return period, P_R , can be calculated as a function of the number of years in the period of interest, Y , and the desired probability of exceedance, P_{EY} , using the formula,

$$P_R = \frac{-Y}{\ln(1 - P_{EY})}$$

$Y = 50$ years, $P_{EY} = 10\% = 0.10$. Substituting and solving

$$P_R = \frac{-50}{\ln(1 - 0.10)} = 475 \text{ years}$$

The -year return period for the desired loss equates to an annual frequency of exceedance of $1/475$ years or 0.0021 per year. For the case of Figure 2 with this annual probability of non-exceedance, the associated repair cost is found as \$8.75M. This represents **91.63%** of the building's total replacement cost. Likewise, as shown in the Figure 2, the average annual repair cost come to **\$85210.2717**.

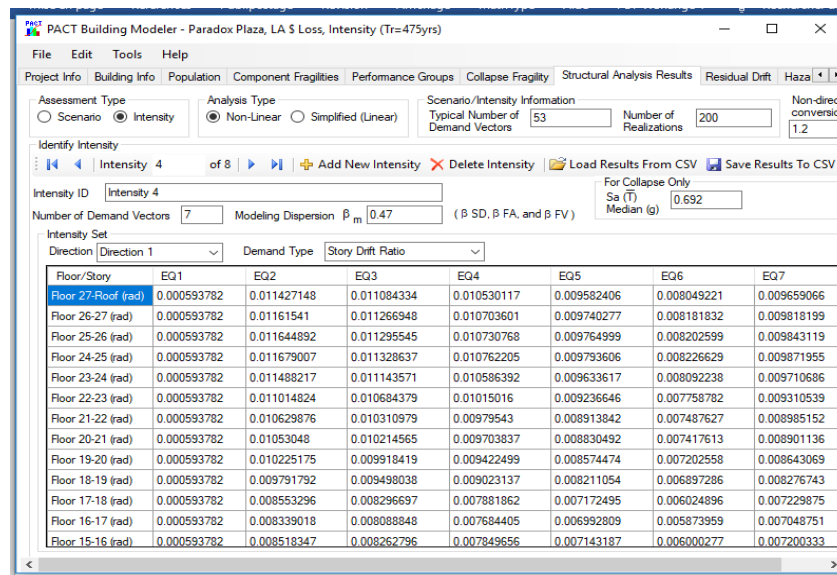
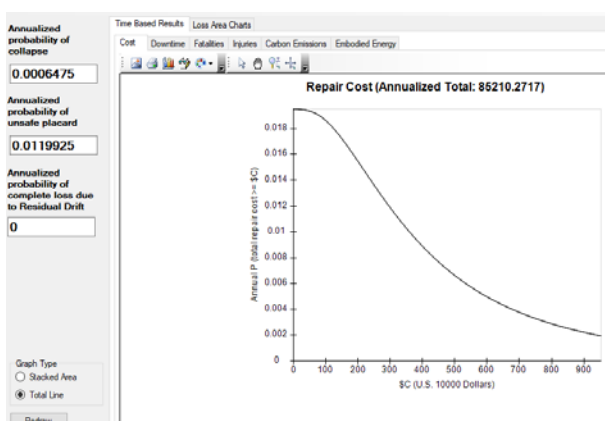
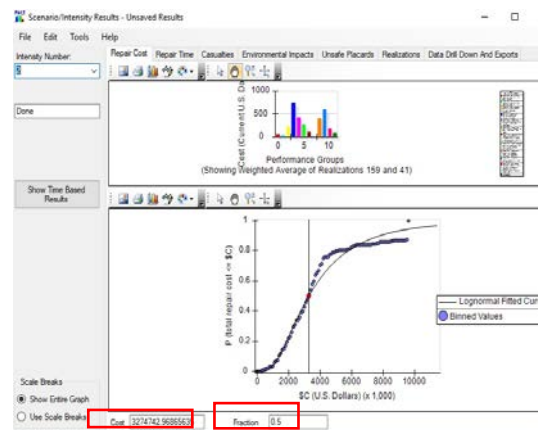


Figure 24. Structural Analysis Results tab with drift input for intensity 4



(a)




(b)

Figure 25. Time Based Results tab showing annualized repair cost figure (a), figure (b) shows the Scenario/Intensity Results tab showing repair cost. (50% is seen as likely repair costs of \$ 3,274,742.96.

USRC Rating Range for New Regulation Compliant Building

This certification method (USRC) Rating, you live in, you do the building work that defines the expected disaster or investment performance. Building certification level of the repair cost, depending on the injury and repair time again is shaped into groups of 5 stars as shown in figure 26.



Safety	Damage	Recovery
5★ Injuries and blocking of exit paths unlikely	5★ Minimal damage (< 5%)	5★ Immediately to days
4★ Serious injuries unlikely	4★ Moderate damage (< 10%)	4★ Within days to weeks
3★ Loss of life unlikely	3★ Significant damage (< 20%)	3★ Within weeks to months
2★ Loss of life possible in isolated locations	2★ Substantial damage (< 40%)	2★ Within months to a year
1★ Loss of life likely in the building	1★ Severe damage (40%+)	1★ More than one year
NE Not Evaluated	NE Not Evaluated	NE Not evaluated

Figure 26. Rating USRC-class table that we use in this study evaluated the building according to the degree USRC 3 *.

REDI Rating Range for New Regulation Compliant Building

The figure 27 shows the RED grading of certificate which is building repair costs, repair time and injury due to "Platinum, Gold, Silver" offers Certificate, in 3 main groups.

Platinum	<p>Downtime: Immediate Re-Occupancy (Green Tag expected) and Functional Recovery < 72 hours</p> <p>Direct Financial Loss: Scenario Expected Loss < 2.5%</p> <p>Occupant Safety: Physical injury due to failure of building components unlikely</p>
Gold	<p>Downtime: Immediate Re-Occupancy (Green Tag expected) and Functional Recovery < 1 month¹</p> <p>Direct Financial Loss: Scenario Expected Loss < 5%</p> <p>Occupant Safety: Physical injury due to failure of building components unlikely</p>
Silver	<p>Downtime: Re-Occupancy < 6 months (Yellow Tag possible) and Functional Recovery < 6 months¹</p> <p>Direct Financial Loss: Scenario Expected Loss < 10%</p> <p>Occupant Safety: Physical injury may occur from falling components (but not structural collapse), fatalities are unlikely</p>

Figure 27. RED Grid Rating Class calculated in the study building is silver certified according to this rating system.

6. Results and Discussion

In this study, a new generation risk assessment analysis has been carried out for a highrise building which was analyzed by traditional methods and performance calculations.

The FEMA P58 methodology which is one of the new generation risk assessment approach has been applied. The existing structural and non-structural fragility curves have been used for a sample highrise building and the repair cost, repair time, injuries and insurance cost of the building have been calculated probabilistically. It is believed that the results of this study will be valuable for building owners, managers, insurance companies, and risk management.

The analysis results obtained in the study are as follows:

- According to TBDY 2018, the target highrise building has provided the “Collapse Prevention ” performance level under the DD1 earthquake level.
- After the performance analysis, the new generation resilience based risk assessment analyzes have been carried out according to FEMA P58. The cost and duration losses for the structural and non-structural members have been determined. The loss results have been graded according to the independent rating agency USRC and REDI. 3-Stars and Silver categories have been assigned respectively.

The study demonstrated the necessity of resilience based assessment evaluating the building with not only structural but also non-structural elements. This approach is considered valuable in terms of providing predictive measures with the approximate calculations such as the cost and time required to return to normal life, beyond ensuring life safety in the building after the earthquake.

TBDY 2018 earthquake regulation allows us to predict the expected behavior of the structural member of the buildings after the possible earthquake. However operators, employers, and builders now demand more than that. In the content of new generation regulations, it is revealed that analysis of cost and time losses should be considered after possible earthquake.

Based on these results, seismic risk identities of structures and regions can be created according to USRC (US Resiliency Council and REDI (Resilience-based Earthquake Design Initiative), which are international rating agencies

REFERENCES

[1] USRC: US Resiliency Council (2016)

[2] REDI: Resilience-based Earthquake Design Initiative (ARUP)

[3] P58 FEMA (2002): Next-Generation Building Seismic Performance Assessment Methodology, RO

[4] Sir MPSO's Hamburgers Gumpertz & Heger Inc., San Francisco, CA, USA, CA. Rojahn and Jim Heintz Applied Technology Council, Redwood City, CA, USA, MG Mahoney Federal Emergency Management Agency, Washington, DC, USA

[5] FEMA P-58-1 (2018), Seismic Performance Assessment of Buildings Volume 1 - Methodology Prepared by APPLIED TECHNOLOGY COUNCIL 201 Redwood Shores Parkway, Suite 240 Redwood City, California 94065 www.atcouncil.org

[6] Djima W.G., Zulfikar C. and Tuzun C., (2019), Performance Based Design for Healthcare Facilities, International Civil Engineering and Architecture Conference, 17-20 April 2019, Trabzon, Turkey

[7] FEMA P-58-2 (2018), Seismic Performance Assessment of Buildings Volume 2 - Implementation Guide Prepared by APPLIED TECHNOLOGY COUNCIL 201 Redwood Shores Parkway, Suite 240 Redwood City, California 94065 www.atcouncil.org

[8] ACI (2008) Building Code Requirements for Masonry Structures and Specifications for Masonry Structures, ACI-530-08, ASCE 5-08 / TMS 402-08 (2008), Masonry Standards Joint Committee of the American Concrete Institute, American Society of Civil Engineers, and the Masonry Society, Farmington Hills, Michigan

[9] Toprak E., (2019), Deprem sonrası bina ve tesis kullanımında olası süre kayıplarının deđerlendirilmesi ve alınabilecek önlemler (in Turkish), Presentation at the Chamber of Civil Engineers Istanbul Branch, 29-30 May 2019,

[10] ACI (2011), Building Code Requirements for Structural Concrete and Commentary ACI 318-11, American Concrete Institute, Farmington Hills, Michigan

[11] ASCE, (2002), Minimum Design Loads for Buildings and Other Structures, ASCE / SEI 7-02, the American Society of Civil Engineers, Reston, Virgin

[12] PEER Ground Motion Database (Pacific Earthquake Engineering Research Center), <https://ngawest2.berkeley.edu/>